



Wood-Supported cationic polyelectrolyte membranes from a reactive ionic liquid for water detoxification

Muzamil Jalil Ahmed^{a,b}, Antoni Sánchez-Ferrer^{a,*}

^a Wood Materials Science, Wood Research Institute of Munich (HFM), Technical University of Munich, Winzererstrasse 45, 80797 Munich, Germany

^b Thin-Film Lab, Advanced Materials and Sustainable Environment (AMSE) Group, NED University of Engineering and Technology, Main Campus, University Road, Karachi 75270, Sindh, Pakistan

ARTICLE INFO

Keywords:

Reactive ionic liquids
Glycidyltriethylammonium chloride
Wood Quaternisation
Cationic polyelectrolytes
Water Treatment

ABSTRACT

Quaternised Wood Membranes (QWMs) are gaining prominence as cost-effective, sustainable alternatives for water detoxification, particularly the removal of hazardous oxoanions such as nitrate (NO_3^-), sulfate (SO_4^{2-}), and phosphate (PO_4^{3-}). Pinewood has been quaternised using a polyelectrolyte-forming reactive ionic liquid (RIL), *i.e.*, glycidyl triethylammonium chloride (GTEAC), in a water-free, one-step method. The optimised modification process at 90 °C and for 1.5 h results in a substantial increase in the oxoanion removal efficiencies of the QWMs, with the most effective removal being achieved for SO_4^{2-} , followed by PO_4^{3-} and NO_3^- . The GTEAC can polymerise to yield long-chain cationic polyelectrolytes, which corroborates with a model synthetic study, the 1D and 2D NMR spectra, and the DSC and TGA/DTG thermal analyses. This grafted polyelectrolyte yields a high weight gain $w_g = 40\%$ and the corresponding degree of quaternisation of $\text{DQ} = 2.08 \text{ mmol/g}$, though screening effects yield a maximum ion exchange capacity of $\text{IEC}_{\text{max}} = 1.07 \text{ mmol/g}$. Additionally, the regeneration is feasible after several filtration cycles and the QWM can withstand sufficient stress under operation conditions. Further, isothermal analyses indicate a Langmuir behaviour and Freundlich-like behaviour under equilibrium (zero flow) and flow conditions, respectively. This study highlights the potential of QWMs as a sustainable and cost-effective alternative to synthetic polymeric membranes in water treatment technologies for denitrification, desulfurisation, dephosphatisation and/or ultrafiltration applications. The process sustainability was quantified using the Eco-Scale approach of up to 73.6 (near excellent), yielding wood-based AEMs costing 50–60 times less than their synthetic polymeric peers.

1. Introduction

Certain oxoanions, such as the nutrient NO_3^- , SO_4^{2-} , and PO_4^{3-} ions and those of toxic heavy metals, can accumulate in surface waters from agricultural runoff, and municipal and industrial waste [1,2]. Further risk is associated with eutrophication, hypoxia (O_2 depletion), algal blooms, and microbial accumulation in developing countries' potable and commercial water streams [3,4]. Fluctuations in water supply can be averted if existing greywater or non-potable water could be reused or reutilised, should these be treated to remove said excess of NO_3^- , SO_4^{2-} , and PO_4^{3-} in addition to other metallic oxoanions [5]. Anion removal applications to date are based on electrocoagulation, and adsorption by using ion exchange systems and electromembrane separation techniques [6–8].

Lignocellulosic materials, *e.g.*, wood-based materials, offer a cost-

effective, abundant feedstock for developing versatile, functional ion exchange applications [9,10]. Extensive efforts on acquiring individual components such as cellulose from lignocellulosic sources increase manufacturing costs due to hydrolysis, derivatisation and cumbersome chemical modifications [11,12]. However, to date, chemical modifications for wood-derived lignocellulosic membranes have been attempted extensively using expensive, often less available chemical modifiers [11]. In this regard, ionic liquids (ILs), have become increasingly popular in wood and cellulose chemistry given their use as green solvents, control over product distributions, reactivity, catalyst immobilisation and recycling [13]. Moreover, nucleophilic addition reactions have been reported for certain Brønsted-basic ionic liquids containing methylimidazolium and quaternary ammonium groups [14]. Notwithstanding, the use of versatile, cost-effective modifiers, such as reactive ionic liquids (RILs), offers an interesting approach to wood modification, *e.g.*,

* Corresponding author.

E-mail address: sanchez@hfm.tum.de (A. Sánchez-Ferrer).

<https://doi.org/10.1016/j.cej.2024.158841>

Received 9 November 2024; Received in revised form 19 December 2024; Accepted 20 December 2024

Available online 22 December 2024

1385-8947/© 2024 The Author(s). Published by Elsevier B.V. This is an open access article under the CC BY license (<http://creativecommons.org/licenses/by/4.0/>).

quaternisation or sulphonation [15,16]. The polymerisation reaction of certain ILs such as imidazoliums, pyridiniums and pyrrolidiniums has been reported which can yield long-chain cationic polyelectrolytes [17]. Such features could prove essential in providing for developing functional materials with high ion exchange capacity.

Wood quaternisation – regardless of species – has predominantly been performed using the aqueous alkaline solution of 3-chloro-2-hydroxypropyltrimethylammonium chloride (CHPTAC) [18]. This CHPTAC reagent is subsequently converted to a glycidyl trimethylammonium chloride (GTMAC) by $\text{NaOH}_{(\text{aq})}$, though subsequently leading to rapid hydrolysis of the GTMAC to diol, and several enolic products [18,19]. Thus, this necessitates a direct water-free synthesis for a glycidic RIL that is safer and cheaper to produce with a liquid quaternary amine, e.g., the reaction between triethylamine (TEA) and epichlorohydrin (ECH). The use of these RILs is also limited to the development of wood polymer composites [16], electrochemically conductive wood [20], and wood preservation [21]. Moreover, wood modification using a water-free RIL-based method is also scarcely reported. Contemporary glycidic-RIL methods incur high hydrolysis loss and lower functionalisation efficiency of the wood's biopolymers. Nevertheless, applications in oxoanion separation have rarely been thoroughly investigated.

Softwoods offer an inexpensive, low-density, green scaffold for producing functional materials for various applications. The presence of nano- and microscale pores, as well as small cavities, e.g., tracheids, rays and parenchyma, in such softwood scaffolds, is crucial for filtration [22]. Wood's unique anatomical structure, its porous microstructure, e.g., pits, tracheids, vessels and fibres, and cell wall biopolymers can contribute to substantial filtration effects. Previous research has shown that wood filters from different wood species can easily remove nanoparticles, bacteria, protozoa and microplastics with high efficiencies (>99%) with a size exclusion > 160 nm governed by the pit's aperture, though low molar mass dyes of <1 nm show fairly substantial removal efficiencies (<65%) via self-diffusion through the cell wall [23].

Jiao *et al.* (2020) reported an ultrafiltration application of multi-layered wood membranes for removing organic pollutants, e.g., dyes, and heavy metals at high adsorption efficiencies (99%) [24]. The use of wood or modified wood offers an interesting avenue for ultra/nano-filtration and ion exchange. The latter is characterised by the ion exchange capacity (IEC), i.e., the ability of a charged functional group to displace its counter ion, e.g., OH^- ions against NR_4^+ groups [25]. For instance, Douglas fir wood chips were modified with GTMAC, a common wood quaternisation agent prepared from the glycidation of CHPTAC by $\text{NaOH}_{(\text{aq})}$. The resulting quaternised wood membranes (QWMs) possessed a high IEC = 1.86 mmol/g [26]. GTMAC was used to prepare Balsa wood QWMs with high cationic conductivity and improved ion transport properties [20]. Densified, epoxy-reinforced, GTMAC-based and carboxylated birch membranes were recently reported for reverse electro-dialysis (RED) purposes [27]. GTMAC-based QWMs have also been proposed as salinity-gradient reverse electro-dialytic membranes for power generation from sea and river water [28].

The above state-of-the-art implies that the wood's micro- and nanostructure properties for size exclusion, ultra-filtration and molecular adsorption could be fine-tuned by using the appropriate RILs that can readily impregnate and functionalise the wood's biopolymers, e.g., cellulose, hemicelluloses and lignin. Moreover, 'true' wood-based anion exchange membranes (AEMs) in literature are scarce, e.g., in denitrification, desulfurisation and dephosphatisation applications. In contrast to polymeric membranes, using quaternised wood as a potential substitute offers comparative ion exchange and ultrafiltration capabilities at much-improved cost-effectiveness and sustainability. Using novel RILs, such as glycidyl triethylammonium chloride (GTEAC), offers an interesting approach to water-free, neutral pH wood modification that significantly reduces processing steps and helps keep the wood cell walls integrity. We further report a polymerisation reaction of the GTEAC that can form cationic polyelectrolytes grafted to the wood biopolymers.

Their effects have also been investigated, *esp.* in their impact on the QWM performance and ion exchange capacity. Thus, the present work aims to develop wood-based AEMs demonstrating oxoanion-removing capabilities.

2. Materials and methods

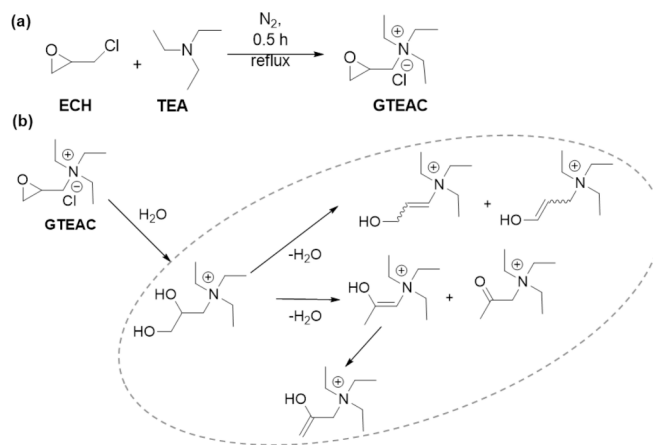
2.1. Materials

Filter discs (50 mm \varnothing) were cut from 2 mm thick, 60 \times 60 mm² wooden slabs in two orthotropic directions, i.e., longitudinal (L) and tangential (T). The wooden slabs were taken from pinewood (*Pinus sylvestris* or Scots pine). The pinewood (PW) filter discs were first dried at 110 °C for ca. 2 h in a convection oven. Epichlorohydrin (ECH; 99%, ThermoFisher Scientific, Germany) and triethylamine (TEA; 99.7%, Sigma-Aldrich, Germany) were used as received. Sodium hydroxide (NaOH), sodium chloride (NaCl), sodium nitrate (NaNO_3), sodium sulphate (Na_2SO_4), disodium hydrogen phosphate (Na_2HPO_4) and all other salts, reagents and auxiliary chemicals were all procured from Merck kGaA, Germany. Deionised water was used for the quaternised wood membrane (QWM) washing and filtration, whereas all analyses disclosed have used solutions prepared from MilliQ Type 1 (ultrapure) water (conductivity: 0.055 $\mu\text{S}/\text{cm}$). All feed solutions based on NO_3^- and SO_4^{2-} were at neutral pH excluding the feed PO_4^{3-} solution which was kept at pH > 12 ($\text{pK}_a = 12.4$, i.e., 50% HPO_4^{2-} and PO_4^{3-}). The concentrations of said feeds and their respective permeates were spectrophotometrically determined using HI93728-01, HI93751-01 and HI93713-01 chromogenic reagents (Hanna Instruments Ltd., Romania).

2.2. Methods

2.2.1. Glycidyltriethylammonium Chloride (GTEAC) Synthesis

ECH was reacted with TEA in a 1:1 M ratio, with a 5% excess of the second, under reflux at 100 °C for 35 min in a silicone oil bath (Scheme 1a). 30.00 g (0.324 mol) ECH and 34.45 g (0.340 mol) TEA were reacted in a 100 mL two-neck round-bottom flask with a condenser under a nitrogen atmosphere, with constant vigorous stirring (450–500 rpm). The reaction yielded a slightly transparent mixture comprising GTEAC and dense oil-like droplets at the end of the reaction. The oil phase which is mostly composed of water-soluble enolic degradation products (Scheme 1b) was separated from the supernatant phase. The remaining liquid, GTEAC, was to be stored at temperatures <10 °C to slow down the degradation that forms a slightly viscous oil due to the presence of any moisture. Yield: 58.91 g (91.5%) GTEAC. ¹H NMR (400 MHz, CDCl_3): $\delta = 3.34\text{--}3.22$ (1H, m, CH_2N), 3.15 (1H, dd, CH_2N , $J =$



Scheme 1. (a) Reaction scheme for the synthesis of GTEAC. (b) Byproducts formed during the GTEAC synthesis due to the presence of trace water molecules.

7.17–7.24 Hz), 2.90–2.80 (1H, m, CH), 2.54–2.46 (1H, m, CH₂), 2.30 (1H, dd, CH₂, $J = 2.47$ and 4.89 Hz), 2.13 (6H, q, CH₂-CH₃, $J = 7.17$ Hz), 0.64 (9H, t, CH₂-CH₃, $J = 7.21$ Hz) ppm. ¹³C NMR (100 MHz, CDCl₃): $\delta = 50.9$ (CH₂), 46.3 (CH), 45.9 (CH₂CH₃), 44.5 (CH₂N), 11.3 (CH₂CH₃) ppm. FTIR (ATR): 2962 (st, CH₃), 2790 (st, CH), 1464 (b, NEt₃⁺), 1377 (b, gem-CH₂), 1209–1273 (st, CH₂), 1064 (st, C-O-C), 843–736 cm⁻¹ (st, C-Cl) cm⁻¹. Further details regarding the individual spectral characterisation (FTIR-ATR and NMR) for TEA and ECH are provided in the Supporting Information (AD SI-1 and Fig. S1). The 2D NMR for the GTEAC are provided in Figs. S2–S5 in the Supporting Information.

2.2.2. Model Synthesis for the Cationic Polyelectrolyte – poly-GTEAC

The model poly-GTEAC with a degree of polymerisation DP = 13 was synthesised via a solventless, chain-growth polymerisation using *n*-butanol as an initiator at 90 °C for 1.5 h and under a nitrogen atmosphere (Scheme 2a). ¹H NMR (400 MHz, CDCl₃): $\delta = 3.54$ (d, $J = 5.4$ Hz, 2H, CH₂-O), 3.20 (tdd, $J = 5.4, 3.9, 2.5$ Hz, 1H, CH), 2.86 (dd, $J = 4.8, 3.9$ Hz, 2H, CH₂-N), 2.48 (q, $J = 7.1$ Hz, 6H; CH₃CH₂-N), 0.99 (t, $J = 7.2$ Hz, 9H, CH₃CH₂-N); 2.65 (dd, $J = 4.8, 2.5$ Hz, 2H, CH₂O(Bu)), 1.57–1.46 (m, 2H, CH₂(Bu)), 1.45–1.29 (m, 2H, CH₂(Bu)), 0.90 (t, $J = 7.4$ Hz, 3H, CH₃(Bu)). ¹³C NMR (100 MHz, CDCl₃): $\delta = 62.38$ (CH₂O(Bu)), 54.54 (CH₂-O), 51.33 (CH₂-N), 45.02 (CH-OR), 34.98 (CH₂(Bu)), 19.04 (CH₂(Bu)), 13.94 (CH₃(Bu)), 11.73 (CH₂CH₃). The 1D and 2D NMR data are provided in Figs. S6–S9 in the Supporting Information. The resulting polymer was further characterised by DSC and TGA/DTG. The degree of polymerization was calculated from the ¹H NMR spectrum using the ratio between the area of the methyl group ($\delta = 0.99$ ppm, 3H, t, CH₃) of *n*-butanol and the area of the methyl group ($\delta = 2.48$ ppm, 9H, t, CH₃) from the ethyl moiety of the ammonium group and resulting into a value of DP = 13.

2.2.3. Wood Quaternisation using GTEAC

The QWM filters in the L-direction were prepared according to the variations described in Table 1. Briefly, PW discs (50 mm ϕ , 505 \pm 10 kg/m³, L-direction), were dried in an air convection oven (Memmert, Germany) for 1 h at 110 °C, weighed, and the GTEAC was added in a 12-wt ratio. The modification reaction was performed in air-tight glass containers under a nitrogen atmosphere at 90 °C for 1.5 h. After the reaction, the QWM filters were washed with deionised water several times to remove any excess GTEAC or any byproduct from the synthesis. The QWM filters were dried at 65 °C for 2 h and then were preconditioned or charged in 1 M NaCl solution for at least 24 h. The QWM filters

Table 1

Variations in the preparation of QWM filters in the L-direction at different temperatures (T) and reaction time (t) at the constant GTEAC/PW weight ratio of ca. 12. Weight gain percentage (w_g), degree of quaternisation (DQ), and maximum ion exchange capacity (IEC_{max}). All measurements were done in triplicate.

Filter disc	T (°C)	t(h)	w_g (%)	DQ (mmol/g)	IEC _{max} (mmol/g)
QWM L11	60	1	13.5	0.79	0.77
QWM L12	60	1.5	15.6	0.80	0.87
QWM L21	90	1	31.8	1.64	0.96
QWM L22	90	1.5	40.2	2.08	1.07

can be regenerated using the same solution post-recovery. The quaternisation and its impact on both the micro- and nanoscale are schematically illustrated in Scheme 2b and Fig. 1. Reaction outcomes were characterised using the changes in the dry weight of the original PW filters, i.e., the weight gain percentage (w_g), the number of quaternary ammonium sites (N_Q) in the QWM filters and the degree of quaternisation relative to initial weight (DQ), as follows:

$$w_g = \frac{w - w_0}{w_0} \times 10 \quad (1)$$

$$DQ = \frac{N_Q}{w_0} = \frac{(w - w_0)}{w_0 M_{GTEAC}} \quad (2)$$

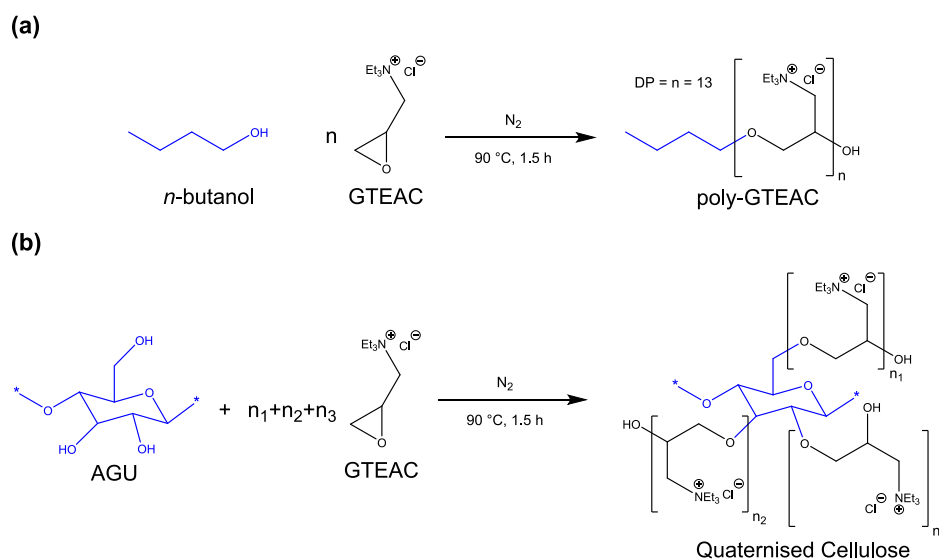
where w_0 and w correspond to the initial and final dry weights of the PW and QWM filters, respectively, and M_{GTEAC} is the molar mass of the GTEAC (C₉H₂₀NOCl: 193.72 g/mol). The DQ is the maximum number of binding sites or the number of quaternary ammonium (RNEt₃⁺) groups grafted onto the wood biopolymers.

2.2.4. Fourier-Transform Infrared Spectroscopy (FTIR) spectroscopy

Fourier-Transform Infrared Spectroscopy (FTIR) spectra were recorded using a Nicolet iS50 FT-IR spectrophotometer (ThermoFisher Scientific) with an attenuated total reflection (ATR) accessory (diamond/ZnSe crystal). Spectra were recorded in the range of 4000–500 cm⁻¹ and were measured at a spectral resolution of 4 cm⁻¹ and averaged over 32 scans.

2.2.5. Nuclear Magnetic Resonance (NMR) spectroscopy

¹H and ¹³C nuclear magnetic resonance (NMR) spectra were



Scheme 2. (a) Synthesis of poly-GTEAC from the GTEAC monomer and *n*-butanol as an initiator at 90 °C for 1.5 h under a nitrogen atmosphere. (b) Ideal quaternisation reaction and grafting of the cationic polyelectrolyte (poly-GTEAC) with the anhydrous glucose unit (AGU) from cellulose.

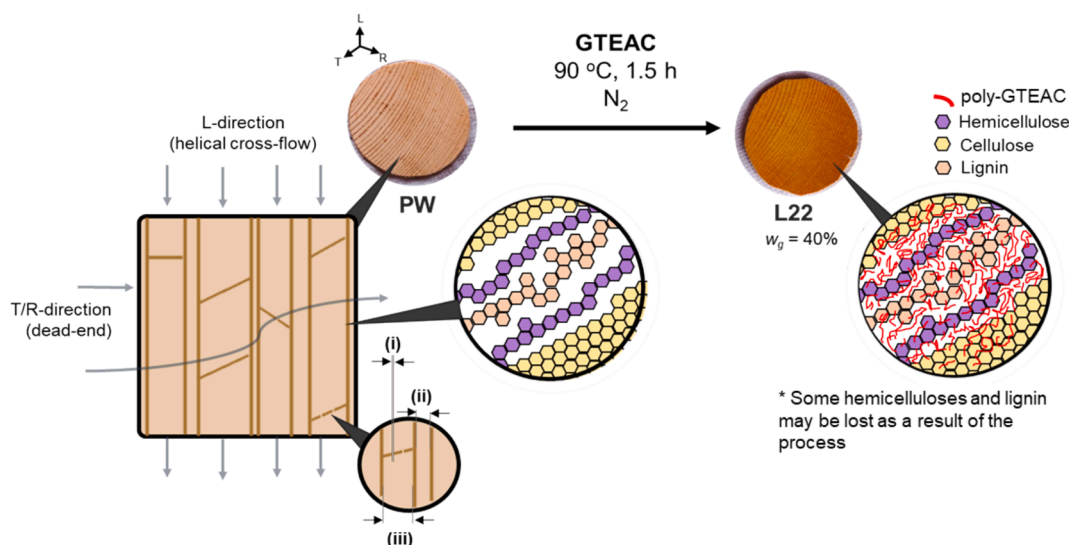


Fig. 1. (a) Overview of the PW modification towards the production of QWM filters, with inset figures corresponding to the theorised changes in the micro- and nanostructure of the wood, indicating diameters of (i) the pits – $6 \pm 2 \mu\text{m}$, (ii) tracheids (earlywood) – $45 \pm 15 \mu\text{m}$, and (iii) tracheids (latewood) – $45 \pm 35 \mu\text{m}$. Data reproduced from ref. [41].

recorded using a 400.13 MHz Bruker (AVHD400) Avance-III (Bruker BioSpin GmbH, Germany), and CDCl_3 (99.8% D; VWR, the Netherlands) was used as a solvent at 25°C . The NMR Spectra were processed and analysed using MestReNova 14.2.1. (Mestrelab Research Lab S.L, Spain). ^1H NMR spectra were recorded with at least 64 scans with a 5.0 s relaxation delay, 4.09 min acquisition time and pulse width 14.5° . ^{13}C NMR spectra were recorded with at least 256 scans with a 3.0 s relaxation delay, 1.157 min acquisition time, spectral width 28.409 Hz and pulse width 9.7° . 2D NMR techniques such as ^1H - ^1H correlation spectroscopy (COSY); ^1H - ^{13}C heteronuclear single-quantum correlation spectroscopy (HSQC), ^1H - ^{13}C heteronuclear multiple-quantum correlation spectroscopy (HMBC), and nuclear Overhauser effect spectroscopy (NOESY) were performed to validate the GTEAC structure assignments in the 1D spectra. HSQC and HMBC were recorded using 8 scans, 2.0 s relaxation delay, 14.5 ppm of spectra width, 0.21 min acquisition time and 1024×1024 -time domain data points ($F2 \times F1$). All parameters were the same for COSY and NOESY except 4 scans were recorded over a 0.29 min acquisition time across 1024×512 -time domain data points ($F2 \times F1$).

2.2.6. Mass and Volume Swelling

Samples ($10 \times 10 \text{ mm}^2$; L-direction) were taken from PW and QWM filters. These samples were first dried at 30°C in a drying oven for 6–8 h. until constant dry membrane mass (m_0) and were equilibrated in water at room temperature for *ca.* 24 h. The pieces were then surface dried by removing surface water using cotton wipes, and weighed, to obtain the wet membrane mass (m) [26,29]. The mass swelling parameter q_m is the ratio between the wet membrane mass (m) to the dry membrane mass (m_0):

$$q_m = \frac{m}{m_0} \quad (3)$$

The volumetric change was further investigated with respect to the sample length L , width b , and thickness h after equilibrating in water. This volume change was estimated from the volume swelling parameter q_v as the overall product of the ratios between the final and initial dimensions, *i.e.*:

$$q_v = \frac{L}{L_0} \frac{b}{b_0} \frac{t}{t_0} = \frac{V}{V_0} \quad (4)$$

2.2.7. Ion Exchange Capacity

The ion exchange capacity (IEC) of the QWM filters or the number of charged functional groups per mass of the dry membrane was determined spectrophotometrically based on the difference between the number of moles of NO_3^- in the permeate n_p and the feed n_f . This IEC evaluation corresponds to removal experiments. The relation is given as:

$$\text{IEC} = \frac{n_p - n_f}{w_0} \quad (5)$$

The concentration of NO_3^- from the permeate and the feed was spectrophotometrically measured using a HI97728 Nitrate Photometer ($\leq 130 \text{ mg/L NO}_3^-$ range, $\pm 0.5 \text{ mg/L}$ accuracy, Hanna Instruments, Romania) at the wavelength $\lambda = 525 \text{ nm}$. The photometer uses a chromogenic Cd-based reductant (HI93728-01) that can correlate the NO_3^- concentration with the absorption intensities of the reagent. This spectrophotometric IEC determination is similar to what has been described elsewhere [30]. Thus, the concentration of NO_3^- ions was estimated via a calibration curve (Fig. S10a). The theoretical IEC corresponds to the degree of quaternisation (DQ).

Further, the maximum ion exchange capacity (IEC_{max}) of the QWM filters was estimated under equilibrium (zero flow) conditions. Briefly, $10 \times 10 \text{ mm}^2$ pieces were cut from dried QWM filters, washed with MilliQ water and immersed in 10 mL of 1 M NaNO_3 (aq) for 48 h. After this time, the QWM filter samples were washed again with MilliQ water and immersed in 10 mL of 0.5 M NaCl (aq) solution. The known concentration of NO_3^- released by QWM filter samples was then spectrophotometrically measured (as described above). The amount of displaced NO_3^- ions by the QWM was corrected using the IEC_{PW} and the ratio between the dry mass of PW and QWM (w'_0/w_0)

$$\text{IEC}_{\text{max}} = d_f \frac{C_{\text{NO}_3} V_{\text{NO}_3}}{M_{\text{NO}_3} w_0} - \text{IEC}_{\text{PW}} \frac{w'_0}{w_0} \quad (6)$$

where V_{NO_3} is the known volume of the NO_3^- solution (*i.e.*, 10 mL) and C_{NO_3} is the concentration of displaced NO_3^- (in mg/L), respectively. M_{NO_3} is the molar mass of the NO_3^- ion (62 g/mol), and the d_f is the analyte solution's dilution factor (100 total/stock).

2.2.8. Mechanical Testing

A self-made bending testing machine, equipped with a 100 N load cell was used to perform a three-point bending (3 PB) test. The flexural

stress and strain at failure were determined for test specimens having a length of $L = 60$ mm, a breadth of $b = 10$ mm and a thickness of $h = 2$ mm cut from the QWM filters. The cylindrical supports were placed across a span of $L_0 = 50.1$ mm. The crosshead displacement rate was $dD/dt = 0.6$ mm/min. For rectangular homogenous material, the obtained values of the applied load F and the crosshead displacement D can be converted into the flexural stress σ and strain ε using the following equations [31]:

$$\varepsilon = \frac{6hD}{L_0^2} \quad (7)$$

$$\sigma = \frac{3FL_0}{2bh^2} \quad (8)$$

The flexural modulus E was determined from the slope of the corresponding stress–strain curve in the linear elastic regime. The 3 PB tests were performed in both the wet and dry (20 °C and 65% RH) states. For the former, the specimens were soaked in deionised water for 24 h prior to testing. The toughness U_T was estimated as the area under the stress–strain curve. The specific strength σ_{sp} values were estimated for comparison between samples at a specific strain value of $\varepsilon_{sp} = 4 \cdot 10^{-3}$ which corresponds to a displacement of $D = 0.8$ cm.

2.2.9. Oxoanion Removal Efficiency

A dead-end filtration assembly (47 mm fritted, 40/35, Glassco, VWR, Germany) was used to test the performance of the QWM filters in oxoanion removal efficiencies η_i where i corresponds to unitary oxoanion feedstocks (*i.e.*, NO_3^- , SO_4^{2-} and PO_4^{3-}) of 30 mg/L concentration. These feedstocks were kept at neutral pH except for the PO_4^{3-} feed (pH 12) – at this pH, the latter feedstock is 1:1 HPO_4^{2-} and PO_4^{3-} . The dead-end filtration was performed *as-is* without the need for an external force under ambient conditions. The oxoanion removal efficiency was calculated as follows:

$$\eta_i (\%) = \left(1 - \frac{n_{p,i}}{n_{f,i}} \right) \times 100 \quad (9)$$

where, $n_{f,i}$ and $n_{p,i}$ refer to the moles of oxoanion i (*i.e.*, NO_3^- , SO_4^{2-} , PO_4^{3-}) removed for the feed and permeate, respectively. The NO_3^- concentration was determined using the Cd-based reduction method described above. The SO_4^{2-} concentrations were determined using the HI97751 photometer (≤ 150 mg/L, ± 5 mg/L accuracy, Hanna Instruments Ltd., Romania) at the wavelength $\lambda = 466$ nm. The technique is based on the turbidity/scattering method using pure anhydrous BaSO_4 (HI93751-01 reagent kit). The PO_4^{3-} concentrations were determined using the HI97713C photometer (≤ 2.5 mg/L, ± 0.04 mg/L accuracy, Hanna Instruments Ltd., Romania) at the wavelength $\lambda = 610$ nm. The technique is based on the ascorbic acid method using the HI93713-01 reagent kit. The concentrations for SO_4^{2-} and PO_4^{3-} were estimated from their corresponding calibration curves (Fig. S10b and c).

The feed volume to membrane volume ratios varied between 12.7 ($50 \text{ cm}^3/3.9 \text{ cm}^3$) and 63.7 ($250 \text{ cm}^3/3.9 \text{ cm}^3$) to ascertain the impact on the η_i performance. The permeate flowrate Q_p (in L/h), filtration time t_f (in h) and the permeate flux J_p (in $\text{L}/(\text{m}^2 \cdot \text{h})$) were estimated for dead-end filtration, considering the constant membrane area of 19.6 cm^2 and thickness $h = 2$ mm. The oxoanion removal efficiency values were further estimated after the QWM filters were recharged in the 1 M $\text{NaCl}_{(aq)}$ solution for 24 h up to 72 h. The loss in membrane mass was also measured. All measurements were performed in ambient conditions.

2.2.10. Ion Exchange Isothermal Analysis (at equilibrium and under flow conditions)

Ion exchange isotherm experiments have been performed using differing concentrations of the oxoanion NO_3^- , *i.e.*, 5–200 mM. The QWM specimens were preconditioned in 1 M NaCl before the experiment, and washed with MilliQ water several times to remove any excess of Cl^- . The

use of IEC at varying concentrations of the oxoanion (*e.g.*, NO_3^- as a model monovalent ion) can provide an ion exchange profile that could be modelled using a Langmuir isotherm in equilibrium conditions or using a Freundlich isotherm under flow conditions. The former behaviour assumes: (1) single-layer ion exchange occurs; (2) the distribution of adsorption sites is relatively homogeneous; (3) the adsorption energy is constant; and (4) the interaction between oxoanions is negligible [55]. The isotherm is given by:

$$\text{IEC} = \text{IEC}_{\text{max}} \frac{K \cdot C}{1 + K \cdot C} \quad (10)$$

where IEC and IEC_{max} are the apparent and maximum ionic exchange capacity, K is the ion exchange constant at equilibrium, and C is the ion concentration at equilibrium. Under flow conditions, this behaviour shifts to a Freundlich-like behaviour. It is reported that the Freundlich isotherm describes a condition where there is a coverage fraction of 50% chemisorption [55]. Both Langmuir and Freundlich isotherms are interrelated in this aspect as elaborated by Halsey and Taylor [56]. The Freundlich isotherm is given as follows:

$$\text{IEC} = \text{IEC}_{\text{max}} (K \cdot C)^n \quad (11)$$

The physical phenomena are based on the simplification of ion exchange interactions as the so-called single ion, homovalent site exchange [32], without or with the influence of flow (alternatively, at or below equilibrium/saturation).

2.2.11. Scanning Electron Microscopy (SEM)

Scanning Electron Microscopy (SEM) images were captured using a Carl Zeiss EVO-40 XVP electron microscope (Carl Zeiss, Germany) to examine the microstructure of the PW and QWM samples.

2.2.12. Thermal Characterisation

Thermogravimetric analysis (TGA) experiments were performed using a TGA50/M3 from Mettler Toledo and controlled by a TC15 TA controller from Mettler Toledo. A small amount of *ca.* 6–8 mg of the samples was placed in standard 70 μL aluminium oxide capsules. Samples were heated from 25 °C to 1000 °C at a 10 K/min heating rate and under a N_2 atmosphere. Differential scanning calorimetry (DSC) experiments were carried out on a DSC 822 calorimeter from Mettler Toledo with an autosampler. A small amount of 5–10 mg of the sample was placed in a 40 μL aluminium pan with a hole. Samples were heated from -50 °C to 200 °C at a 10 K/min heating rate and under a N_2 atmosphere.

2.2.13. EcoScale and Process Technoeconomics

The sustainability of the GTEAC synthesis and the wood modification process has been quantified using the EcoScale Assessment methodology [33]. The post-synthesis assessment assigns cumulative scores after evaluating various material inputs, reaction parameters and experimental setups used and using the so-called penalty tables where the associated risks, hazards and negative impacts of the method parameters are considered. These penalties are subtracted from the maximum score (100) representing an ideal green process to get a value that ranks the synthetic methods in terms of the corresponding green quality (for high-purity products). Additionally, the technoeconomics associated with the QWM filter is also studied.

3. Results and discussion

3.1. Reactive Ionic Liquid (GTEAC) Synthesis

Glycidyltriethylammonium chloride (GTEAC) synthesis was optimised from a reported method from McClure [34], which suggests reacting ECH and TEA in equimolar amounts at 25 °C without any solvent (Scheme 1a). Given the slow glycidation rate due to the TEA's steric hindrance, the reaction temperature was ramped until reflux at > 120 °C

and conducted in a nitrogen atmosphere. Initially, both reagents form a clear transparent mixture that, upon reaching near-total completion, starts to form a slightly turbid liquid product, including oil droplets, *i.e.*, the so-called enolic and diol decomposate (Scheme 1b). Upon cooling to room temperature, the product mixture gradually turns white. This product mixture containing GTEAC and some unreacted TEA was stored at temperatures $<10\text{ }^{\circ}\text{C}$ and under a nitrogen atmosphere to inhibit the formation of the decomposate oil over time due to the presence of moisture that can react with the epoxide moiety.

The purity for the GTEAC has been found to be 94% from the ^1H NMR analysis. The 2D NMR experiments have indicated the correlations that validate the ^1H and ^{13}C NMR assignments (Figs. S1–S5). The isolated yield for GTEAC amounts to 91.5%. The ^{13}C NMR spectra of the GTEAC and the presence of the probable decomposates in Scheme 1b have also been compared (Fig. S11).

3.2. Cationic polyelectrolyte poly-GTEAC Synthesis

Scheme 2a illustrates the polymerisation reaction of the RIL, GTEAC, that yields long-chain cationic or quaternary polyelectrolytes, *i.e.*, poly-GTEAC. NMR characterisation (Figs. S6–S9) reveals that the GTEAC is capable of reacting with molecules containing OH groups (*e.g.*, *n*-butanol and even AGU). The free hydroxyl group of the resulting triethylammonium 2-hydroxypropyl (TEAHP) can further react with another GTEAC and undergo chain-growth polymerisation. The consequences of the production of this cationic polyelectrolyte can be substantial on the substrate material, such as in the present case, PW. The presence of high M_w polyelectrolytes can reduce ion migration, thereby increasing contact time and increasing instances of single-layer homovalent ion exchange or chemisorptive interactions [35]. Based on the peak analyses between CH_3 of the *n*-butanol with that of the RNEt_3^+ side-groups of the polymer chain, yields a degree of polymerisation of *ca.* 13. Arguably, the exposed groups (terminal and middle portions) of this chain are likely to undergo ion exchange, while the effects of the initial grafted units are likely to suffer from a screening or a masking effect [36]. Further discussion regarding the effects of the GTEAC polymerisation are discussed in the following section.

3.3. Wood Modification

The PW quaternisation using the GTEAC is schematically shown in Scheme 2b. The PW specimens were cut into 50 mm \varnothing filter discs, dried and then directly reacted with GTEAC, without the need for wood pre-treatment and swelling step. The avoidance of this step preserves the PW's cell wall scaffold and does not induce loss in mechanical strength for the disc filters, given the low thickness of the discs of 2 mm. Moreover, the wood quaternisation has been performed without the use of the typical aqueous alkaline systems for CHPTAC [20,26,27], which induces hydrolytic decompositions as described in the introduction section. This affects the overall efficiency of the wood quaternisation process and, therefore, the water-free quaternisation performed, herein, yields substantial weight gain, and changes in the physicochemical, mechanical and functional properties of the treated PW. These variations have been observed at varying temperatures and reaction times.

The reaction of GTEAC with the anhydrous glucose unit (AGU) from cellulose is schematically shown in Scheme 2b and effects in Fig. 1. All quaternisation processes have been performed at a 12- wt ratio of GTEAC to the dry PW disc. It is worth noting that the other components in the cell wall, *i.e.*, lignin and hemicelluloses, will also be quaternised during the process. This would explain the colour change in the PW from pine brown to pale yellow–brown due to the modification of the lignin domains (Fig. S12). Similarly, the lignin quaternisation process is well-reported with other commonly used quaternisation reagents, *i.e.*, GTMAC [37,38].

QWM filters in the T-direction were also prepared in the same manner as the L-direction counterparts. Considering the difficulties in

cross-impregnating tangential wood specimens [39,40], the modification time was doubled at the same temperature profiles and an unsuccessful impregnation resulted across the thickness of the sample. QWM filters in the T-direction were prepared at $90\text{ }^{\circ}\text{C}$ for 2 h (T21) and 3 h (T22). These filter disc membranes demonstrated lower w_g values up to 21.2% and 21.1%, respectively. These values correspond to a DQ of *ca.* 1.09 mmol/g. The impregnation has likely happened at the surface and the edges of the tangential filter discs. For this reason, it is recommended that wood quaternisation be performed in the L-direction at the given thickness of $h = 2\text{ mm}$.

The GTEAC is capable of polymerizing (*i.e.*, poly-GTEAC, see experimental details for the synthesis). To better prove the inclusion of such a polymer and to elucidate its nature, DSC and TGA/DTG experiments were performed. Fig. 2a shows the DSC analysis for PW, QWM L22 and poly-GTEAC (DP = 13). The poly-GTEAC has a glass transition temperature of $T_g = 8\text{ }^{\circ}\text{C}$, and the QWM L22 at $T_g = 91\text{ }^{\circ}\text{C}$, while PW has none in this range of temperatures. This increase of the T_g value in QWM is due to the expected higher degree of polymerisation (DP) of the grafted poly-GTEAC in the QWM L22 sample (ratio GTEAC to PW of 12:1) and to the partial immobilization of the polymer chains grafted to the wood biopolymers, *e.g.*, cellulose crystals and lignin network [42,43]. Moreover, from the increase in the heat capacity of the poly-GTEAC of $\Delta c_p = 0.350\text{ J/(g K)}$ and the measured step in the QWM L22 of $\Delta c_p = 0.120\text{ J/(g K)}$, the percentage of grafted polymer can be calculated, resulting into 34% which is close to the 29% calculated from the weight gain of $w_g = 40.2\%$ for QWM L22.

Fig. 2b and 2c show the TGA thermograms and the corresponding derivatives for PW, QWM L22 and poly-GTEAC (DP = 13). The modification with GTEAC leads to a decrease in the decomposition temperature of the wood biopolymers, *i.e.*, from $369\text{ }^{\circ}\text{C}$ to $336\text{ }^{\circ}\text{C}$. The poly-GTEAC has a lower decomposition temperature at $223\text{ }^{\circ}\text{C}$, and upon addition to the PW yields a QWM L22 having said temperature between the two. The addition of amorphous material as poly-GTEAC induces a lower decomposition temperature of the wood biopolymers due to the grafting of such polymers to the accessible hydroxyl groups in the wood cell wall. Similar effects owing to this grafting are well-reported in other reactive polymers based on epichlorohydrin-quaternary amines [44].

Fig. S13a–d shows the SEM images of the PW and the QWM. Given the implications of the use of wood materials as a scaffold, slight yet unsubstantial changes were observed. This signifies that the modification occurs at a molecular level and at conditions where a pore/vessel/void filling effect similar to polymeric membranes cannot be observed. Nevertheless, there exists little observable effect in terms of the increase in the amorphousness (adding-up or filling effects) over the wood surface as shown in Fig. S13c and d. A more definitive proof of the GTEAC modification is attainable by an obvious parameter – the weight gain w_g – which proportionates well with the IEC, the DQ, and the removal efficiencies. The effect of swelling is quantifiable from the swelling parameters q_m and q_v , and further discussion regarding the intrinsic properties and structure of the wooden scaffold is discussed with the oxoanion removal experiments below.

3.4. Physicochemical Properties

The swelling parameters q_m and q_v , and functional properties, *i.e.*, IEC of the QWM filters are important factors that impact their oxoanion removal efficiencies η , as well as the mechanical strength during the ultrafiltration process. The effect of temperature yields unsubstantial changes and the quaternisation time is shown to be much more significant, as observed elsewhere [20,26]. In comparison, the mass swelling parameter of the QWM filters is $q_m = 1.8 \pm 0.1$, while the volume swelling parameter is $q_v = 1.2 \pm 0.1$ (Fig. 3a and Table S1). QWM filters modified at longer reaction times, *i.e.*, QWM L12 and QWM L22, show higher values of both swelling parameters than the corresponding QWM filters produced at shorter times, *i.e.*, QWM L11 and QWM L21, but not too different to those values from PW (*ca.* $q_m = 1.7$ and $q_v = 1.1$). This

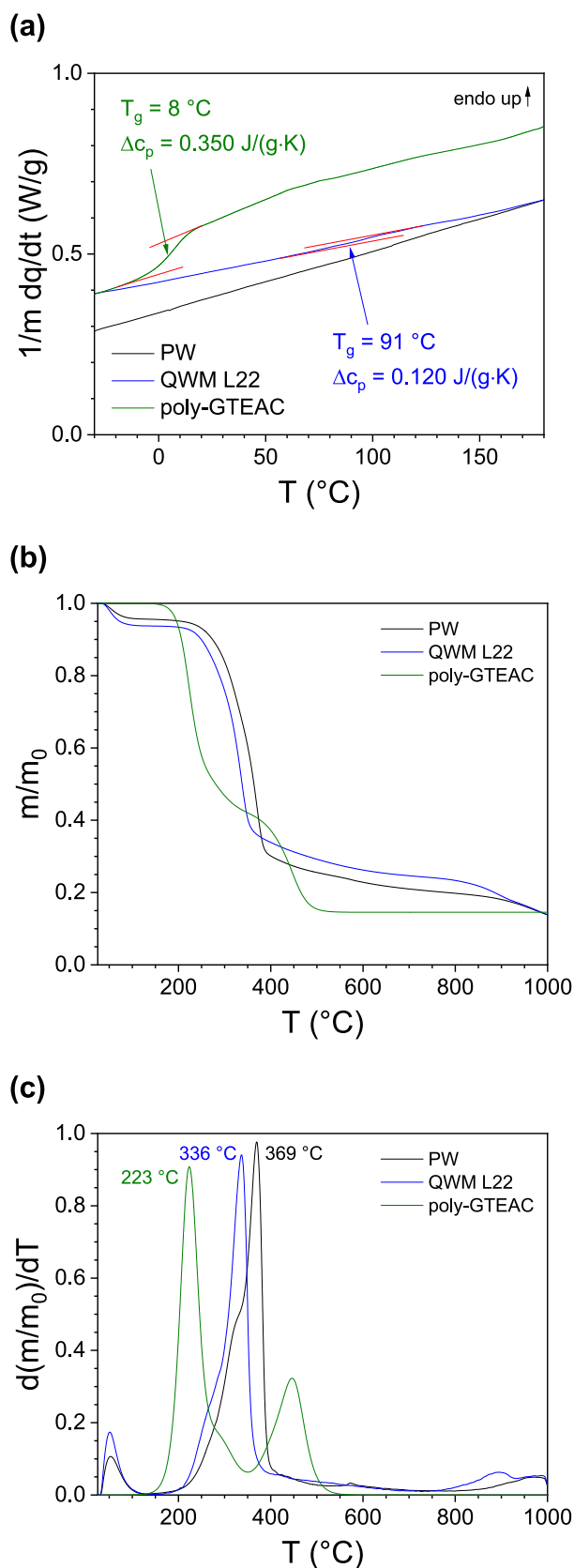


Fig. 2. (a) Differential Scanning Calorimetry (DSC) thermograms, (b) Thermogravimetric Analysis (TGA) thermograms, and (c) the corresponding derivatives to the TGA thermograms for the PW, QWM L22 and poly-GTEAC.

indicates that QWMs do not change too much the affinity for water after the modification process, but the little increase in the swelling effect observed is due to the GTEAC adding into the lignocellulosic cell wall and middle lamella.

The maximum increase in the average density observed for a QWM filter disc deviates from the expected results. For instance, for L22 ($w_g = 40.2\%$), the apparent density is $575 \pm 65 \text{ kg/m}^3$ ($n = 5$) rather than the expected maximum, *i.e.*, 708 kg/m^3 . The deviation in apparent density from the maximum relates to the fact that the GTEAC can induce (i) quaternisation of the lumina-cell wall interface with the corresponding filling up of the lumina with no change in volume ($\Delta V \approx 0$), (ii) quaternisation and swelling of the cell wall biopolymers with the corresponding increase in volume ($\Delta V > 0$), or (iii) both at the same time (Fig. S14). In the first case, a substantial volume of GTEAC ($\rho_{\text{GTEAC}} \sim 1154 \text{ kg/m}^3$) will take up space in the cell wall/lumina interface, *i.e.*, surface filling quaternisation (SFQ). For the second case, if only the lignocellulosic biopolymers in the cell wall are reacted and swollen simultaneously, *i.e.*, bulk swelling quaternisation (BSQ). Generally, these effects can be mathematically described using the following relation:

$$\left(\frac{\rho}{\rho_0}\right)_{\text{swelling}} = \frac{m}{m_0} \frac{V_0}{(V_0 + \Delta V)} \leq \frac{\rho}{\rho_0} \leq \left(\frac{\rho}{\rho_0}\right)_{\text{filling}} = \frac{m}{m_0} \quad (12)$$

where m and m_0 are the mass, V and V_0 , are the volume of the discs after and before modification, respectively, and $\Delta V = (m - m_0)/\rho_{\text{GTEAC}}$.

The maximum ratio between post- and pre-modification densities of the QWM filter disc is given by the ratio ρ/ρ_0 . For the surface filling quaternisation (SFQ) scenario and for the bulk swelling quaternisation (BSQ) situation, an upper limit $(\rho/\rho_0)_{\text{filling}}$ and a lower limit $(\rho/\rho_0)_{\text{swelling}}$ can be estimated. The SFQ and BSQ ratio can be calculated as follows:

$$\text{SFQ} = \frac{(\rho/\rho_0) - (\rho/\rho_0)_{\text{swelling}}}{(\rho/\rho_0)_{\text{filling}} - (\rho/\rho_0)_{\text{swelling}}} \quad \text{and} \quad \text{BSQ} = 1 - \text{SFQ} \quad (13)$$

As shown in Table S1, considering the density ratio for the QWM L22 filter disc lies in the range of $1.21 < (\rho/\rho_0 = 1.33) < 1.40$ ($n = 5$). This amounts to 37% swelling of the cell wall biopolymers (BSQ) and 63% for the lumen/cell wall interface filling (SFQ) by the GTEAC (Fig. 3b). The experimental SFQ values for the four QWM filters, *i.e.*, L11, L12, L21 and L22, were 67%, 50%, 62% and 63%, respectively, whereas the values obtained from the fitting in Fig. 3b were 55%, 65%, 59% and 64%. Therefore, the modification process accounts for a *ca.* 35–40% of bulk functionalisation and 60–65% of surface functionalisation regardless of the modification conditions.

The natural permeability and porosity of the PW scaffold have been retained, if not slightly increased. The PW quaternisation leads to substantial dimensional expansion as well as an increase in mass. It is worth noting that an excessive increase in the q_m (or q_v), can prove detrimental to ion transport and diffusion for ion exchange membranes [45,46]. The swelling for the modified wood pertains to swelling and enlargement of the fibres, tracheids or vessels in the microstructure [47] but only in the amorphous domains. However, the above findings suggest a controlled effect that will not compromise the ion exchange performance of the wood. This implies that the water permeability, dimensional stability and separation efficiency for QWMs such as for L22, could perform feasibly in their intended oxoanion separation and ultrafiltration application.

The increase in the IEC for the QWM filters is relatively proportional to the DQ (Fig. 3c) and is *ca.* 50% of the theoretical DQ value. The IEC_{max} values were observed to increase with higher quaternisation time and temperature by 240% for QWM L22 with respect to QWM L11, due to the increase in w_g . Comparatively, the IEC value observed for the QWM L22 is similar to that observed for GTMAC-based QWMs (0.8–2.1 mmol/g) and quaternised poly(ether ether ketone) QPEEK (0.9 mmol/g) [26,48]. The hydrophilic nature of the GTEAC used, as with any other quaternary agent plays a dominating role in regulating the q_m and q_v of

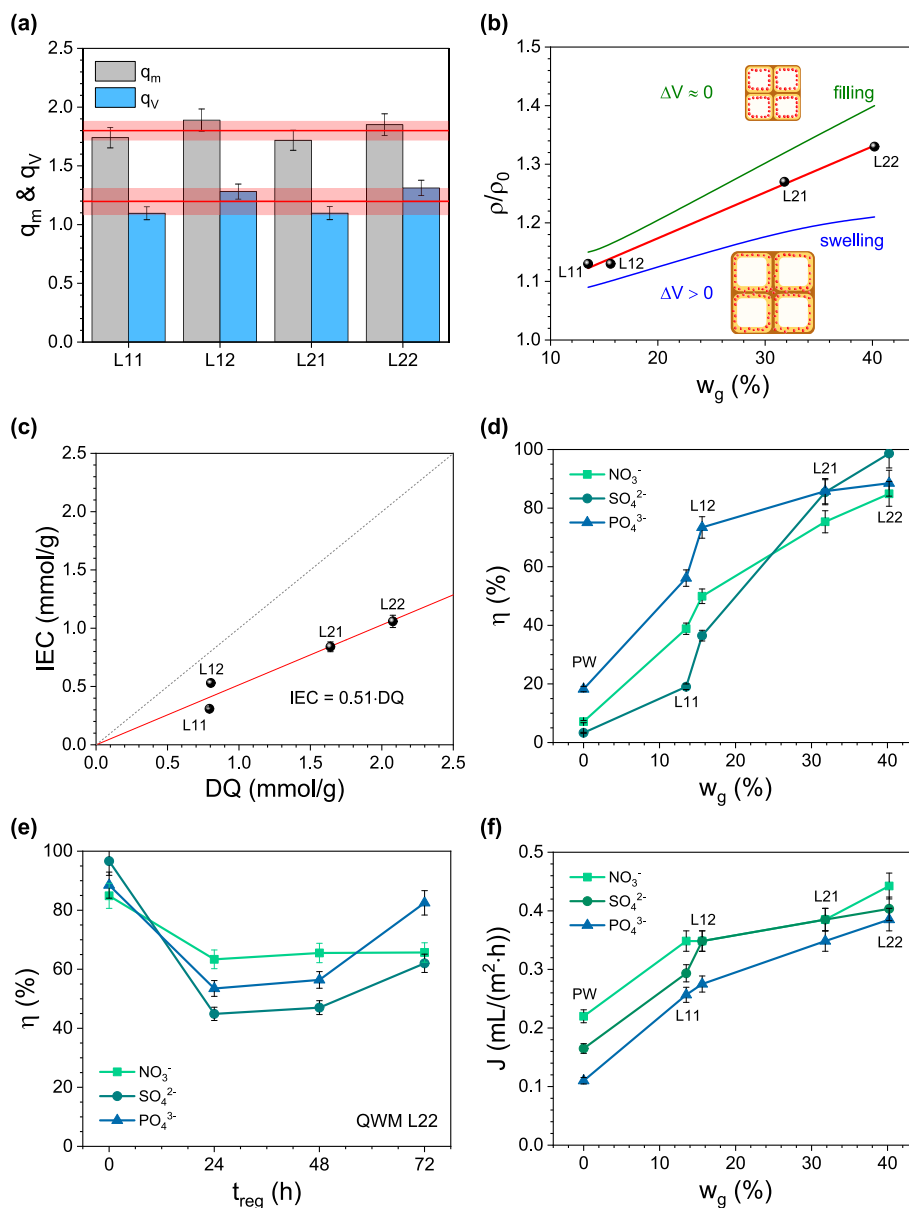


Fig. 3. (a) Mass and volume swelling parameter q_m and q_v , respectively, for the four QWMs (the red line is the average value \pm standard deviation). (b) The density ratio for the four QWMs shows that swelling (BSQ) and filling (SFQ) occur during the modification process. (c) Ion exchange capacity IEC as a function of the degree of quaternisation DQ for the four QWMs. (d) Oxoanion removal efficiencies η for PW and the four QWMs. (e) Post-regeneration removal efficiency η for the QWM L22. (f) Variations in flux J for PW and the four QWMs. (For interpretation of the references to colour in this figure legend, the reader is referred to the web version of this article.)

such QWMs. The hydrated quaternary sites (*i.e.*, $RNEt_3^+$) can form an overlapped solvation shell, which is responsible for the anion transport [46] and limits the percentage of SFQ molecules on the lumen/cell wall interface.

3.5. Oxoanion Removal Efficiency

The removal efficiency of all the modified QWM filters was tested in comparison with the unmodified PW filter, for three target oxoanions, *i.e.*, NO_3^- , SO_4^{2-} and PO_4^{3-} . As shown in Fig. 3d, the unmodified PW filter can remove 7.2%, 3.3% and 18.3% of NO_3^- , SO_4^{2-} and PO_4^{3-} , respectively. The tests were performed using the simple dead-end filtration type glass assembly (Fig. 4a) and values have been reported for the first pass. The QWM filters demonstrated improved oxoanion removal with increasing quaternisation time and temperature. For instance, the QWM L22 filter disc demonstrates considerably improved oxoanion removal efficiency

corresponding to 83.9%, 98.3% and 88.9% of NO_3^- , SO_4^{2-} and PO_4^{3-} , respectively. Increasing quaternisation times and temperature have shown high oxoanion conductivity for certain QWMs [26]. Increasing quaternisation as evident from the DQ values, yields increasing removal efficiency, which is typically observed to be in the order of $SO_4^{2-} > PO_4^{3-} > NO_3^-$. For instance, the increase in quaternisation temperature from 60 °C to 90 °C, demonstrates a removal efficiency for QWM L22 that *ca.* 2–3 times that of L11 and L12. The increase in removal efficiency is also notable for the latter two QWM filters with increasing temperature and time, but the effect of increasing quaternisation time is not as prominent for L21 and L22 (Table S1). The oxoanion removal efficiencies can also be visualised by the colour of the feed and permeate solutions (as a step during the spectrophotometric quantification), as shown in Fig. 4b.

The removal efficiency of the QWM filters tends to decrease following multiple consecutive runs (Table S1), possibly due to gradual fouling and maximum retention of the oxoanions per binding sites of the

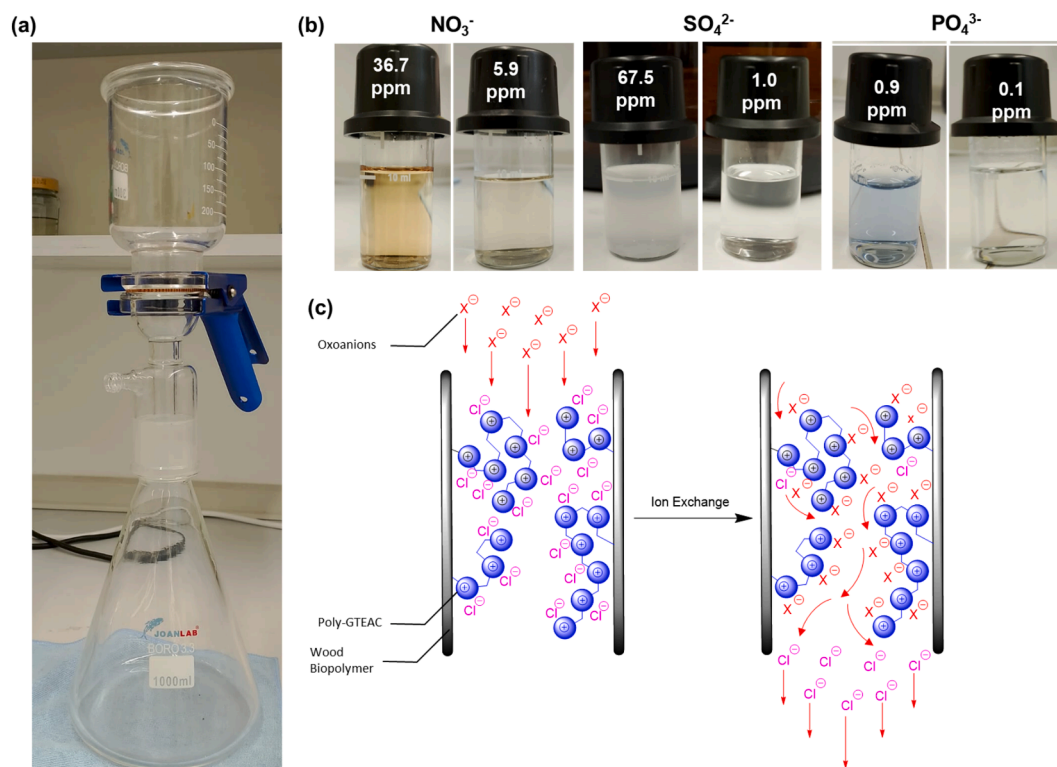


Fig. 4. (a) Ultrafiltration setup for the prepared QWM filters. (b) Changes in the oxoanion concentration. Note that the solution colour is due to the addition of the chromogenic reagents used to determine the exact concentrations spectrophotometrically. (c) Proposed mechanism of the ultrafiltration via the QWM filters.

QWM filters. For this reason, the QWM filters need to be washed with deionised water and recharged in 1 M NaCl solution (regeneration or reconditioning process) for ≥ 72 h to regain their almost original oxoanion removal capacity. The QWM L22 filter demonstrates the most stable post-regeneration recovery for all three oxoanions tested (Fig. 3e). The recoveries are observed to return to their original recoveries after 72 h, except for SO_4^{2-} which requires a longer time. In comparison to the other QWM filters, as shown in Fig. S15, the post-regeneration recoveries are relatively low for QWM L11, L22 and L21, owing to lower quaternisation (or lower number of binding sites). The increase in oxoanion removal efficiency is tied to the obvious increase in the DQ, and IEC or the available quaternary sites in the swollen QWM filters.

Moreover, the flux J for modified the four QWM filters, as evident in Fig. 3f and Table S1, shows the effects of changes in the so-called aqueous feed flow throughput for increasing DQ. The increase in the J pertains to the two possibilities discussed above, *i.e.*, (i) the GTEAC adding onto the lignocellulosic cell wall and/or (ii) filling up the lumina. This is likely to manifest as the swelling of the wood's internal microstructure by channel enlargement which can in turn expand ion transport pathways. The individual PW's intrinsic channels, *i.e.*, tracheids and parenchyma, are retained in the QWM filters. The interconnected tracheids in softwoods such as pine, can act as ion channels. These are usually *ca.* 22 μm for latewood tracheids. For earlywood tracheids, the diameters of such softwood can be *ca.* 35 μm [49]. Complimentary pits range from about 0.1 to 0.5 μm [50]. It is likely that during higher temperatures and time, the cell wall-derived porous membranes (*i.e.*, margo) in the bordering pit pairs are modified. This could lead to the displacement of the valve-like torus under internal pressure due to the intense quaternisation process [51]. This means that the quaternisation procedure can open up new ion transport pathways and lead to improved flux rates and NF/IX capabilities of the QWM filter discs (Fig. 3f).

The effect of varied filter loadings on the removal efficiency (Table S2), *i.e.*, V_f/V_{QWM} of 12.7 ($V_f = 50$ mL) and 63.7 ($V_f = 250$ mL)

was also studied. The latter results in oxoanion removals that are 1.65, 1.07 and 1.14 times lower for NO_3^- , SO_4^{2-} and PO_4^{3-} , respectively. It is, therefore, recommended that a low feed volume of up to 50 mL is maintained for high removal efficiencies for the dimensions of these discs.

Vertically aligned, open ion channels contribute to low tortuosity in the L-direction of the PW and enable lower flow resistances preventing water flow throughput issues. These issues are commonly observed for packed activated carbon filters or granular particle filters [24]. The triethylammonium 2-hydroxypropyl (TEAHP) groups are covalently bonded to the cell wall biopolymers, which then undergo grafting with GTEAC molecules to give long-chains of cationic polyelectrolyte containing quaternised ammonium RNEt_3^+ groups. This can form a sort of coating over the PW's existing ion channels, and can thus act as capillary columns. This effectively enables the QWM filter to remove oxoanions selectively or simultaneously in terms of their hydration radius R_h . The R_h for the oxoanions, NO_3^- , SO_4^{2-} , PO_4^{3-} (and HPO_4^{2-}) is said to be 0.18 nm [52], 0.30 nm, and ~ 0.2 nm [52–54], respectively. The progressive increase in the R_h incurs significant effects on the corresponding oxoanion removal, *i.e.*, $\text{SO}_4^{2-} > \text{PO}_4^{3-} > \text{NO}_3^-$. This effect is also observed for the other QWM filters. The SO_4^{2-} removal/retention is higher than PO_4^{3-} owing to the hydration effects of the latter oxoanion. This owes to the fact that the latter can speciate to HPO_4^{2-} and PO_4^{3-} oxoanions, despite a larger radius of hydration R_h for these two oxoanions. Upon appropriate quaternisation – such as the case for QWM L22, the cationic polyelectrolyte with RNEt_3^+ functionalities act as brush-like tethered cationic groups (Fig. 4c) that can retain said oxoanions *via* the so-called ion transport modes discussed above.

3.6. Ion Exchange Isotherms

Fig. 5a shows the experiments used for the construction of the isotherms under equilibrium (blue symbols) or under flow (green symbols) conditions. All these points fall below the curve of maximum ion

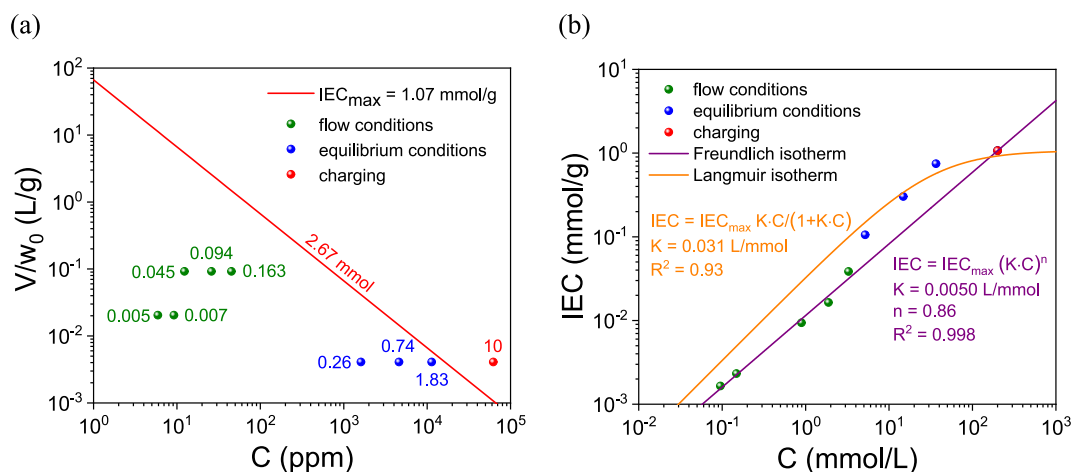


Fig. 5. (a) Log-log plot of weight-normalized head volume vs concentration for the QWM L22. The red line corresponds to the point with the same number of available binding sites (2.67 mmol) of the maximum $IEC_{max} = 1.07$ mmol/g; the blue and green symbols are ionic exchange data in equilibrium and flow conditions, respectively, and the red symbol corresponds to the charging conditions. The numbers for each data point correspond to the maximum binding sites that can be exchanged. (b) Ion exchange isotherms for QWM L22 at 25 °C and ambient pressure under quasi-equilibrium (t_R : 48 h) and under flow (t_R : 0.5 h) conditions. The orange and violet curves correspond to the fitting of the data using the Langmuir and the Freundlich model, respectively. (For interpretation of the references to colour in this figure legend, the reader is referred to the web version of this article.)

exchange capacity $IEC_{max} = 1.07$ mmol/g, therefore, they correspond to removal experiments, while the data in red correspond to the charging of the membrane. Data were fitted either using eq. (10) or eq. (11) for equilibrium or flow conditions, respectively. Fig. 5b shows the fitting to the data under equilibrium conditions (blue symbols; orange fitting curve – eq. (10) and under flow conditions (green symbols; violet fitting curve – eq. (11).

At the maximum IEC_{max} (1.07 mmol/g), the apparent number of binding sites is 2.67 mmol. The oxoanion removal efficiencies will be expected to be > 90–95% when the feed number of moles is lower than this value. In equilibrium conditions, the surface absorption/ion exchange behaviour is dominant [57]. Under flow conditions, vehicular diffusion and Grothuss hopping are dominant mechanisms that occur through the solvated oxoanions by the quaternary ammonium groups [58,59]. The ion exchange constant $K = 0.031$ L/mmol obtained from the data under equilibrium conditions (Langmuir isotherm) implies that this state favours a stronger binding than in the flow state whose exchange constant is $K = 0.0050$ L/mmol. It is known that some specific sites can have a stronger affinity for anions (e.g., NO_3^-) than other sites [60]. This implies that the entanglement of the grafted chains can lead to a masking or suppressing effect of the initial unit grafted to the wood biopolymer, as described elsewhere in the case of flexible polyelectrolytes [36]. This also explains the discrepancy between the theoretical IEC, i.e., $DQ = 2.08$ mmol/g, and the observed IEC_{max} (1.07 mmol/g). Moreover, the exponent value of $n = 0.85$ (heterogeneity factor) indicates a non-linear correlation between the number of mols of anions present during the filtration process and the binding sites due to the fast flow of the feed solution.

As the grafted poly-GTEAC can restrict ion transport across the membrane, esp. in the absence of flux, this can lead to chemisorption which falls under the assumptions of the Langmuir model. This behaviour is described by the single-site homovalent ion exchange with anions, e.g., NO_3^- [32,61]. Yet under flow conditions, we see deviations from this behaviour towards a Freundlich-like isotherm. This effect can be attributed to the relatively lower instance of homogeneity, and uniform distribution of the available quaternary ammonium sites across the polyelectrolyte grafted to the wood biopolymers. In such conditions, the ion exchange occurs across the QWM L22's ion channels and not on the surface – under flow conditions [58]. The cationic polyelectrolyte chains with $RNEt_3^+$ groups are likely to have more affinity for monovalent anions such as NO_3^- [60]. Vehicular transport (standard diffusion) and

Grothuss mechanism (proton hopping) are key features in an anion exchange membrane [59]. The presence of more bulky cationic polyelectrolyte groups can lead to greater overlapped regions that can undergo ion exchange. The presence of longer-chain alkyls leads to more basic nitrogen in GTEAC compared to GTMAC [26].

3.7. Mechanical Properties

3 PB experiments were performed on unmodified PW and the QWM filters in the two coplanar directions, i.e., radial (R) and tangential (T) directions, in either dry or wet conditions. The QWM filters will be subjected to fluid pressure in said directions under filtration conditions. To ascertain the impact of the wood quaternisation process, the flexural modulus E , specific strength σ_{sp} at specific strain ϵ_{sp} , and toughness U_T of the QWM filters in the dry and wet conditions were evaluated, with PW as a reference.

As evident in Fig. 6a-b, QWM L22 samples measured in both the R- and T-direction – the applied force is parallel to the L-direction – show similar flexural modulus values when comparing samples in the dry ($E_{R,dry} = 204$ MPa and $E_{T,dry} = 216$ MPa) and in the wet state ($E_{R,wet} = 193$ MPa and $E_{T,wet} = 124$ MPa), but lower than those from the PW reference samples ($E_{R,dry} = 545$ MPa and $E_{T,dry} = 367$ MPa; $E_{R,wet} = 349$ MPa and $E_{T,wet} = 126$ MPa) where radial bending is dominated by earlywood cell-wall deformation, whereas tangential bending involves latewood layers [62,63]. This softening effect owes primarily to the swelling of the cell wall biopolymers, and levels the flexural modulus values for both directions contrary to the natural PW samples. Therefore, the quaternisation process can lead to the formation of brush-like cationic polyelectrolyte $RNEt_3^+$ -laden cell wall fibres (i.e., swollen fibres) that act as an impurity, and, in the wet state, the loss in flexural modulus relates to the extra plasticisation effect of water.

The softening effect is more evident considering the specific strength σ_{sp} and the toughness U_T , as shown in Table 2. For instance, the corresponding σ_{sp} and U_T for dry and wet QWM L22(R) were 0.81 MPa and 14.4 kPa, and 0.77 MPa and 13.1 kPa, respectively, and almost half of its PW(R) counterpart. Similarly, dry and wet QWM L22(T) samples were 0.77 MPa and 13.1 kPa, and 0.49 MPa and 4.3 kPa, respectively. These findings illicit the fact that (i) in the wet state, water incurs a more plasticising effect than that caused by the cationic polyelectrolyte with $RNEt_3^+$ groups present in the cell wall biopolymers, and (ii) the swelling of said cell wall are core drivers of lower flexural strength or toughness.

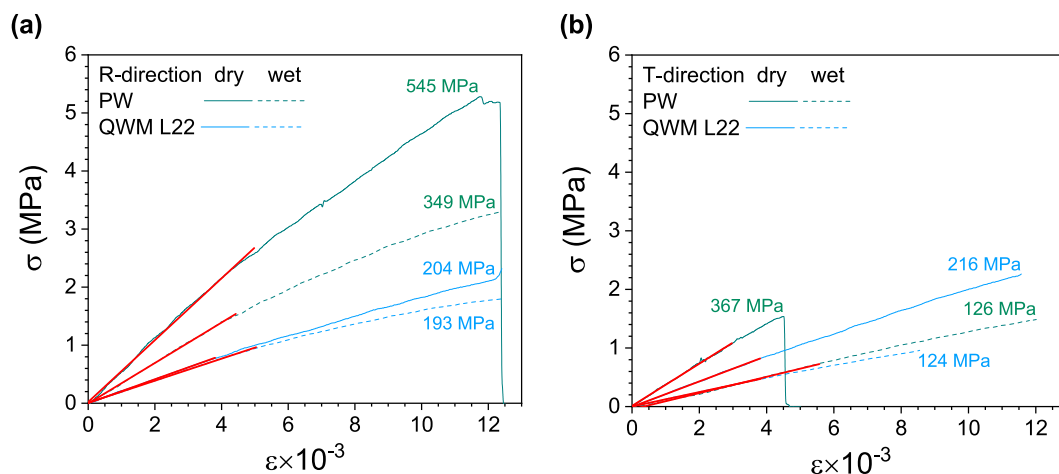


Fig. 6. Stress–strain curves for the unmodified PW sample and the QWM L22 filter ($60 \times 10 \times 2 \text{ mm}^3$), in (a) the R-direction and (b) the T-direction (wet state, dotted line; dry state, solid line). The corresponding flexural moduli are indicated for each curve.

Table 2

Specific strength σ_{sp} , toughness U_T and flexural modulus E for PW and QWM L22 specimens in wet and dry states and in the radial (R) and tangential (T) direction.

Sample	State	Direction	σ_{sp} (MPa) ^a	U_T (kJPa)	E (MPa)
PW	Dry	R	2.16	36.9	545
	Wet	R	1.40	23.5	349
	Dry	T	1.41	3.7	367
	Wet	T	0.52	9.2	126
QWM L22	Dry	R	0.81	14.4	204
	Wet	R	0.77	13.1	193
	Dry	T	0.86	13.7	216
	Wet	T	0.49	4.3	124

^a specific strength at $\epsilon_{sp} = 4 \cdot 10^{-3}$ (equivalent crosshead displacement $D = 0.8$ mm).

In general, the QWM L22 can deform more easily under load/pressure under significant stress, making them more flexible under conventional filtration conditions.

Table 3

Comparison of oxoanion removal efficiencies (i.e., NO_3^- , SO_4^{2-} and PO_4^{3-}) for the QWM filter and other reported materials.

	Process Time (h)	Process Flux (L/(m ² ·h))	Oxoanion Removal Efficiency			Ref.
			$\eta_{\text{NO}_3^-}$ (%)	$\eta_{\text{SO}_4^{2-}}$ (%)	$\eta_{\text{PO}_4^{3-}}$ (%)	
QWM L21 [w]	< 0.5	348–385	75	85	86	This work
QWM L22 [w]	< 0.5	385–440	84	98	89	This work
ZS/PVDF/PEG [pm]	3	500	92	–	99	[67]
Neosepta AMX [pm]	7	1293	82	89	–	[66]
Selemon AMV [pm]	7	1293	85	90	–	
FumaSep FAB [pm]	7	1293	84	50	–	
PS-PPH ₃ [pr]	1.5	6278–7751 ^a	90–95	–	–	[68]
PS-PBU ₃ [pr]	1.5	6278–7751 ^a	90–95	–	–	
SIQA/PVDF [np]	1.2	35	90	–	80	[69]
Hardwood Ppy-AC [w]	24	245	–	82	–	[70]
NF270 [pm]	3	285	–	99.7	–	
CPA2 [pm]	3	285	–	99.8	–	[71]
BPEI-GTMAC Peat [w]	24	– ^b	58	43	–	[72]
Modified Amberlite MB9L [pr]	2	– ^b	57	3	100	[73]
CQAPSU-3.1 [pm]	2.6	14,333	–	–	98	
CQAPSU-3.0 [pm]	5.3	14,333	–	–	93	[74,75]
Anammox EBR [ad]	1.8	400 ^c	79–89	–	93–95	[76]
Octolig® (5 cm bed) [pr]	< 0.5	9600	72	5–42	40–87	
CCNF [w]	< 0.1	6	96	70	61	[65]
GWP Kork-deko [w]	72	63 ^d	29–98	–	–	[77]
GCP Kork-deko [w]			4–8			

Notes: [w] wood- and wood-based materials, [pm] polymeric membranes, [pr] polymeric resins, [ad] anaerobic digestion using anaerobic anammox bacteria, e.g., *nitrosoammonas*; ^a 1-bed volume (BV) = 5.0 mL resin and column: 12 mm ϕ ; ^b batch absorption experiment; ^c bed: 12 mm ϕ , 5 L cycle per batch. ^d granulated cork pellets (2 mm size, 123 kg/m³) and wetland wood pellets (6–8 mm size, 650 kg/m³), bed: 84 mm ϕ , 10 L cycle per batch.

such nanopapers was 0.6 mmol/g [65]. Thus, our method offers high DQ values with appreciable and competitive IEC values for the modified PW, with little amounts of byproduct coming from the RIL synthesised. Moreover, there exists a possibility to recycle the used quaternisation agent for another modification batch. The use of PW as a scaffold material yields sustainable, self-supporting modified wood membranes (QWMs) that can prove substantial in extensive ion exchange/ultrafiltration systems by themselves or as guard/pre-filters for oxoanion removal (*i.e.*, NO_3^- , SO_4^{2-} and PO_4^{3-}).

The oxoanion removal of QWM L21 and QWM L22 has been compared to other QWMs in Table 3 against other denitrification, desulphurisation and dephosphatisation systems, *i.e.*, commercial and reported polymeric membranes, modified resins and related wood-based materials. The QWM L22 possesses a balanced oxoanion removal performance in contrast to its peers, for shorter process time and lower flux. While most resin-, membrane- and nanoparticulate-based denitrification, desulphurisation and dephosphatisation possess higher fluxes and higher time to remove the oxoanions. Considering commercial AEMs, the QWM L22 has comparable removal efficiencies for NO_3^- and

improved efficiency for SO_4^{2-} , though this is achieved at a lower flux and longer time [66].

Higher than optimal fluxes can lead to membrane fouling and reduced removal efficiency due to insufficient contact time [78]. Thus, the QWM L22 may be better positioned to face lesser biofouling and provide for higher throughput. Commercial membranes have densities almost twice that for QWM L22, *e.g.*, AMV and FAB have densities of 1100 and 1200 kg/m^3 , respectively. The IEC and water content per dry membrane λ for AMV, AMX and FAB membranes are also comparable to that of the QWM L22 [66,79,80]. For other wood-based materials based on activated carbon (AC) or impregnated woods such as polypyrrole-activated carbon, the performance for QWM L22 is more significantly enhanced in comparison. In the case of wood carbonisation, despite the so-called retention of nanochannels, the higher porosity and the low ion-conductive properties of the polypyrrole hamper strong electrostatic interactions necessary for oxoanion retention [70].

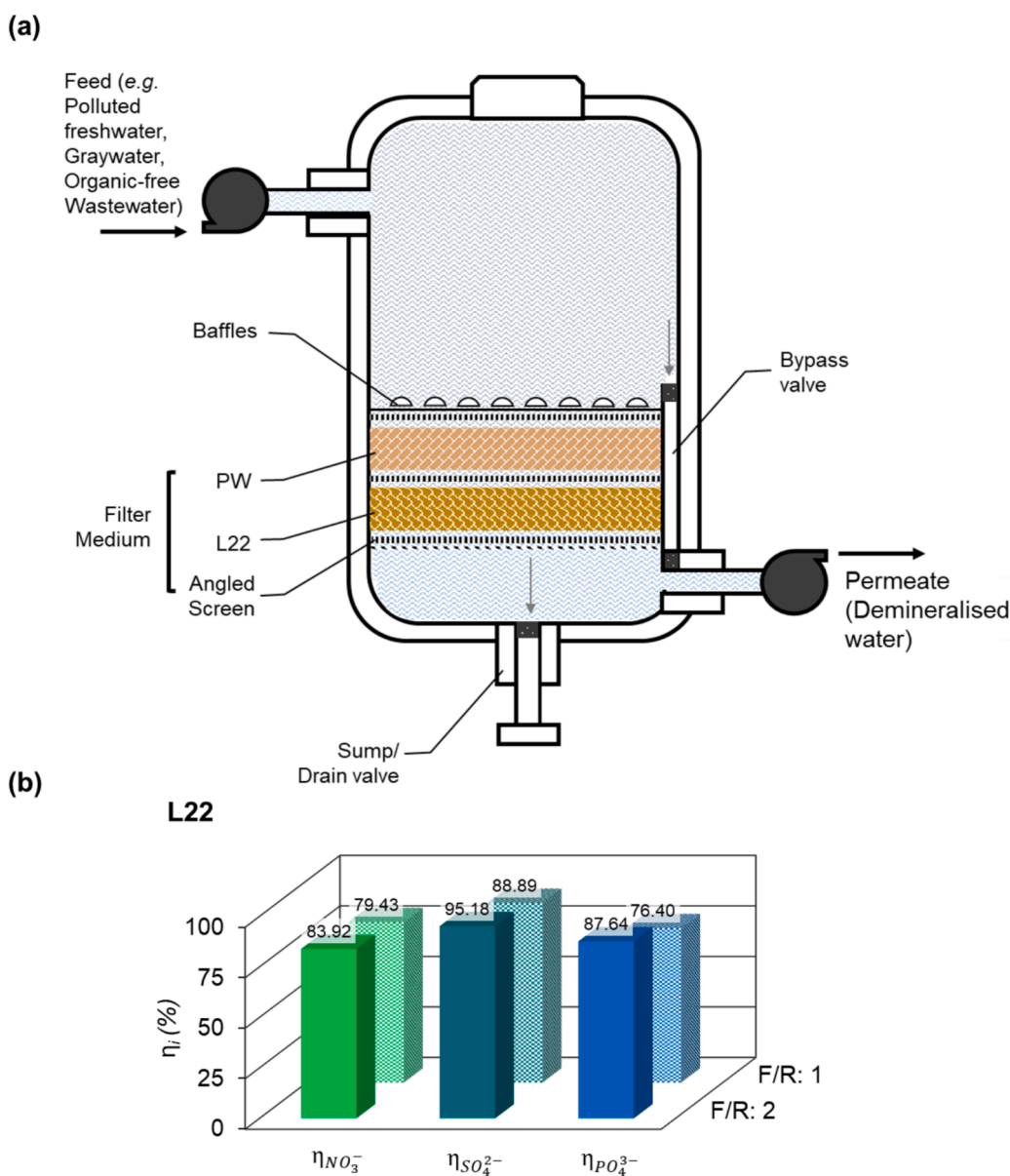


Fig. 7. (a) Proposed oxoanion removal and ultrafiltration bed-type unit for processing large quantities of polluted freshwater and wastewater. (b) Changes in η_i of QWM L22 prepared using 2:1 and 1:1 fresh-to-recycled GTEAC quaternisation reagent.

3.9. Technoeconomic Significance of QWM NF/IX Process

The QWM L22 offers a low-density, relatively efficient oxoanion-removing AEM for denitrification, desulphurisation and dephosphatation purposes. The cost for one L22 filter disc (50 mm ϕ , 2 mm, \sim 540 kg/m³) is estimated to be 3.33–4.12 €/kg or 4.16–5.15 €/m² (Table S3), accounting for electric and material inputs. In contrast to commercially available AEMs such as AMX costs 50–60 times more – ca. 277 €/m² [81]. Moreover, the basic cost of the GTEAC amounts to 0.85–1.27 €/kg (Table S3), which is considerably inexpensive compared to the GTMAC precursor, CHPTAC (60% w/w) which costs 91 €/kg; or the GTMAC (technical, \geq 90%): 4270 €/kg (US/EU) or 324–405 €/kg (China, PR). Thus, the GTEAC synthesis offers a more facile, inexpensive access to a wood impregnation and quaternisation RIL process, which can also be used for lignocellulosic fibres.

The World Health Organisation (WHO) mandates in its Safe Drinking Water Guidelines 2011 that the acceptable levels of NO₃⁻ and PO₄³⁻ as <11 mg/L (ppm) and <0.2 mg/L (ppm), respectively. In the case of SO₄²⁻, their presence is not regulated and should be kept below <250 mg/L (ppm) to avoid aesthetic loss in drinking water or lower to prevent interference or treatment unit degradation [82,83]. The QWM L22 demonstrates to this effect near standard efficiencies in the removal of said oxoanions. Given, that the PW provides for an effectively inexpensive scaffold for wood quaternisation. The size of the QWM L22 filters could be upscaled to make mono- or multilayered filter trays, e.g., large bed-type oxoanion removal and ultrafiltration purposes, or guard filtration units (Fig. 7a). The baffle and screens could assist in distributing the feed across the filters, and the unmodified PW act as a guard filter which can filter out nanoparticulate and particulate matter above 160–490 nm [23]. For beds equipped with QWMs of greater thickness, a pressure-driven wood quaternisation would have to be applied to ensure consistent w_g and DQ values with the GTEAC. This could potentially drive reaction costs and incur greater safety and maintenance expenses.

3.10. Process Sustainability – EcoScale Assessment

The sustainability score for the preparation method of the GTEAC and the QWMs can be quantified using the EcoScale Assessment. The details of penalty calculations for the wood modification are given in Table S3. The penalty data for the synthesis parameters, material inputs and experimental setup is taken from Van Aken *et al.* [33]. The use of ECH and TEA incurs considerable safety risks (penalties), though their limited use per kg dry PW minimises the inherent risks. Nevertheless, the Eco-Scale score for both the GTEAC synthesis and the QWMs preparation amounts to 73.6, which corresponds to well-acceptable or near-excellent reaction scores (*i.e.*, \geq 75) [33].

The wood modification process (Fig. S16) incurs low auxiliary reagents and solvent consumption other than the washing steps for the QWM filters, e.g., QWM L22. The resulting effluent could be recycled or stripped of the GTEAC decomposate or reused. The GTEAC oily decomposate is a primary byproduct waste of the process during the wood modification process and is formed when GTEAC reacts with the residual water in the PW and decomposes at high temperature. The material and energy inputs are not intensive and provide a low-energy, cost-effective method of producing said filters (Fig. 7a). This can prove feasible for setting up larger-scale filtration beds using the QWM L22 in developing world economies facing water scarcity. The disposal of these wood-based filters is either by composting or by regenerating/remodifying the filters (similar to ion exchange resins) upon extensive usage.

The used quaternary RIL reagent, GTEAC, forms two distinctive layers in the reaction vessel, after the wood modification reaction for 1.5 h, where for instance, ca. 19% to 25% of the original reagent GTEAC gets hydrolysed to the decomposate. The decomposate can easily be separated from the remaining quaternary RIL reagent, though the former possesses a slight yellowish discolouration. Nevertheless, the

remaining RIL can be reused for another wood modification in a 1:1 or 2:1 ratio with fresh GTEAC. This yields similar w_g for the specified time and temperature for QWM L22 filters prepared this way (Fig. 7b). The washing steps for the QWM filters require copious amounts of deionised water (ca. 0.7 L to 1.0 L for QWM L22) to remove the excess GTEAC and its decomposate in the wood during the process.

4. Conclusion

This study demonstrates the successful quaternisation of pine wood (PW) using a water-free, sustainable process via a reactive ionic liquid (RIL), GTEAC, prepared via a one-step, non-aqueous, non-alkaline method. The grafting of a RIL has yielded quaternised wood membranes (QWMs) for anionic exchange membranes (AEMs) production such as QWM L22 with high DQ (2.08 mol/kg), and IEC_{max} (1.07 mmol/g) values. The IEC is half the theoretical value, which corroborates with the nearly 4:6 quaternisation of the cell wall biopolymers (bulk swelling quaternisation, BSQ) and filling of the lumen/cell wall interface (surface filling quaternisation, SFQ). Process parameter variations in temperature and reaction time had a profound impact on the physicochemical properties of the wood-based AEMs. Higher temperatures and extended reaction times optimised the membrane's quaternisation process, leading to improved IEC, swelling behaviour, and superior oxoanion removal performance. The optimal conditions – at 90 °C for 1.5 h – produced a QWM L22 with substantial filtration efficiency, making it highly competitive for industrial-scale water treatment applications.

These modifications enabled the wood-based AEM to achieve high removal efficiencies of 83.9% for NO₃⁻, 98.3% for SO₄²⁻, and 88.9% for PO₄³⁻. The performance of QWMs in removing oxoanions is dependent on the hydration radius R_h of the target ions, with larger and more hydrated ions being removed more effectively. However, the case of PO₄³⁻ is an exception where the high hydration energy and thus higher solvation reduces ion transport and mobility – in comparison to SO₄²⁻ and NO₃⁻. The water-free quaternisation process eliminates and preserves the native wood scaffold which would otherwise be highly alkaline environments as reported for GTMAC-modified wood-based AEMs. The quaternisation process is likely to have impacted the wood structure and its mechanical strength, particularly because of the swelling of the cell wall biopolymers and the lumen-cell wall interface filling by the GTEAC. For instance, in the R- or T-direction, the QWM L22 membrane withstands lower strength and toughness than untreated PW, with enhanced deformation capacity due to the quaternisation process.

Given the reaction conditions in which the PW was reacted, it is likely that there is a reaction between the triethylammonium hydroxypropyl – TEAHP – group anchored to the wood biopolymers with another GTEAC molecule, leading to grafted cationic polyelectrolyte RNET₃⁺ chains. This effect can lead to chain mobilities and effects that could be distinguished from thermal data, e.g., T_g increase of the poly-GTEAC as compared to QWM and, therefore, this QWM has a lower decomposition temperature than its PW counterpart, because of the inclusion of a grafted polymer. The implications for this grafting effect can lead to long chains, where only the exposed charges of the grafted polymer sites can undergo ion exchange. The remnant site interaction will progressively decrease with the oxoanions. This explains why our IEC_{max} < DQ under equilibrium and under flow conditions, and that the high weight gain w_g reflects the occurrence of the grafting effect.

The modified ion channels (the interconnected tracheids) can provide for sufficient interactions between the available quaternary ammonium sites and the oxoanions to attain Langmuir behaviour in the steady-state/zero flow or equilibrium conditions. The ion exchange process under zero flow follows a Langmuir behaviour whereas under flow the behaviour shifts to a Freundlich-like isotherm. Furthermore, the QWM L22 membrane retained structural integrity and functionality after multiple regeneration cycles, with minimal performance loss, demonstrating excellent potential for repeated use in water detoxification. These attributes make the QWMs a highly promising alternative to

conventional synthetic membranes, with significant potential for practical applications in denitrification, desulphurisation, and dephosphatation processes. Overall, the cost-effectiveness, sustainability (EcoScale: 73.6), and stable performance of these membranes indicate their feasibility for large-scale water treatment and environmental remediation.

The results from this study suggest that wood-based anion exchange membranes (AEMs) could prove vital for water purification by offering a sustainable and cost-effective alternative to synthetic membranes. Future research could explore scaling up this technology for industrial use in large-scale water treatment plants, focusing on improving the regeneration process and enhancing the long-term durability of the membranes. Additionally, the approach could be expanded to target other contaminants or even different functionalisation methods (i.e., anionic RILs rather than the current cationic one). The Utility of the QWM L22 could be attempted with emerging pollutants such as perfluoroalkyl sulfonates (PFAS), viruses, microplastics and pharmaceutical residues. The development of AEMs from other abundant lignocellulosic materials could further optimise the performance and cost-efficiency, making this technology a versatile solution for global water scarcity challenges, particularly in developing regions.

CRedit authorship contribution statement

Muzamil Jalil Ahmed: Writing – original draft, Visualization, Investigation, Funding acquisition, Formal analysis, Data curation, Conceptualization. **Antoni Sánchez-Ferrer:** Writing – review & editing, Visualization, Validation, Supervision, Software, Resources, Methodology, Investigation, Formal analysis, Data curation, Conceptualization.

Declaration of competing interest

The authors declare that they have no known competing financial interests or personal relationships that could have appeared to influence the work reported in this paper.

Acknowledgements

MJA wholeheartedly acknowledges the support received from the Deutscher Akademische Austauschdienst (DAAD) in the form of the Short-term Research Grant 57693450 (Forschungstipendien – Kurzstipendien 2024/25) to conduct this research. MJA further acknowledges the technical support received from the technical staff of the Wood Materials Science group at the Wood Research Munich (Holzforschung München) and the Bayerische NMR Zentrum (BNMRZ) of the Department of Chemistry at the Technical University of Munich. MJA and TSF further thank Anja Vieler for her assistance in the SEM Characterisation of the PW and QWMs.

Appendix A. Supplementary data

Supplementary data to this article can be found online at <https://doi.org/10.1016/j.cej.2024.158841>.

Data availability

Data will be made available on request.

References

- [1] M. Devlin, J. Brodie, Nutrients and Eutrophication, in: 2023: pp. 75–100. https://doi.org/10.1007/978-3-031-10127-4_4.
- [2] I.U. Din, S. Muhammad, I. ur Rehman, Heavy metal(loid)s contaminations in soils of Pakistan: a review for the evaluation of human and ecological risks assessment and spatial distribution, *Environ. Geochem. Health* 45 (2023), <https://doi.org/10.1007/s10653-022-01312-x>.
- [3] M. Fida, P. Li, Y. Wang, S.M.K. Alam, A. Nsabimana, Water Contamination and Human Health Risks in Pakistan: A Review, *Expo. Heal.* (2022), <https://doi.org/10.1007/s12403-022-00512-1>.
- [4] A. Waseem, J. Arshad, F. Iqbal, A. Sajjad, Z. Mehmood, G. Murtaza, Pollution Status of Pakistan: A Retrospective Review on Heavy Metal Contamination of Water, Soil, and Vegetables, *Biomed Res. Int.* 2014 (2014) 1–29, <https://doi.org/10.1155/2014/813206>.
- [5] M.A.P. Mahmud, F. Ejeian, S. Azadi, M. Myers, B. Pejic, R. Abbasi, A. Razmjou, M. Asadnia, Recent progress in sensing nitrate, nitrite, phosphate, and ammonium in aquatic environment, *Chemosphere* 259 (2020), <https://doi.org/10.1016/j.chemosphere.2020.127492>.
- [6] S. Al-Marri, S.S. AlQuzweeni, K.S.H.R. AlKhaddar, P. Kot, R.S. AlKizwini, S. L. Zubaidi, Z.S. Al-Khafaji, Ultrasonic-Electrocoagulation method for nitrate removal from water, *IOP Conf. Ser. Mater. Sci. Eng.* 888 (2020), <https://doi.org/10.1088/1757-899X/888/1/012073>.
- [7] R.K. Abdulkhader, A.J. Jael, The Use of Electrocoagulation to Remove Fluoride, Nitrates and Phosphorous from Water, *IOP Conf. Ser. Earth Environ. Sci.* 877 (2021) 012021, <https://doi.org/10.1088/1755-1315/877/1/012021>.
- [8] N. Pismenskaya, K. Tsygurina, V. Nikonenko, Recovery of Nutrients from Residual Streams Using Ion-Exchange Membranes: Current State, Bottlenecks, Fundamentals and Innovations, *Membranes (basel)*. 12 (2022) 497, <https://doi.org/10.3390/membranes12050497>.
- [9] N.A.A. Qasem, R.H. Mohammed, D.U. Lawal, Author Correction: Removal of heavy metal ions from wastewater: a comprehensive and critical review, *Npj Clean Water* 4 (2021) 52, <https://doi.org/10.1038/s41545-021-00144-z>.
- [10] S. Periyasamy, V. Karthik, P. Senthil Kumar, J.B. Isabel, T. Temesgen, B. M. Hunegnaw, B.B. Melese, B.A. Mohamed, D.-V.-N. Vo, Chemical, physical and biological methods to convert lignocellulosic waste into value-added products. A review, *Environ. Chem. Lett.* 20 (2022) 1129–1152, <https://doi.org/10.1007/s10311-021-01374-w>.
- [11] M. Mergbi, M.G. Galloni, D. Aboagy, E. Elimian, P. Su, B.M. Ikram, W. Nabgan, J. Bedia, H. Ben Amor, S. Contreras, F. Medina, R. Djellabi, Valorization of lignocellulosic biomass into sustainable materials for adsorption and photocatalytic applications in water and air remediation, *Environ. Sci. Pollut. Res.* 30 (2023) 74544–74574, <https://doi.org/10.1007/s11356-023-27484-2>.
- [12] M.J. Ahmed, J. Ashfaq, Z. Sohail, I.A. Channa, A. Sánchez-Ferrer, S.N. Ali, A. D. Chandio, Lignocellulosic bioplastics in sustainable packaging – Recent developments in materials design and processing: A comprehensive review, *Sustain. Mater. Technol.* 41 (2024) e01077.
- [13] O.S. Hammond, A.-V. Mudring, Ionic liquids and deep eutectics as a transformative platform for the synthesis of nanomaterials, *Chem. Commun.* 58 (2022) 3865–3892, <https://doi.org/10.1039/D1CC06543B>.
- [14] S. Chowdhury, R.S. Mohan, J.L. Scott, Reactivity of ionic liquids, *Tetrahedron* 63 (2007) 2363–2389, <https://doi.org/10.1016/j.tet.2006.11.001>.
- [15] T.J. Szalaty, Ł. Klapiszewski, T. Jesionowski, Recent developments in modification of lignin using ionic liquids for the fabrication of advanced materials—A review, *J. Mol. Liq.* 301 (2020) 112417, <https://doi.org/10.1016/j.molliq.2019.112417>.
- [16] M. Odalanowska, A. Skrzypczak, S. Borysiak, Innovative ionic liquids as functional agent for wood-polymer composites, *Cellulose* 28 (2021) 10589–10608, <https://doi.org/10.1007/s10570-021-04190-1>.
- [17] A. Eftekhari, T. Saito, Synthesis and properties of polymerized ionic liquids, *Eur. Polym. J.* 90 (2017) 245–272, <https://doi.org/10.1016/j.eurpolymj.2017.03.033>.
- [18] Y. Song, Y. Sun, X. Zhang, J. Zhou, L. Zhang, Homogeneous Quaternization of Cellulose in NaOH/Urea Aqueous Solutions as Gene Carriers, *Biomacromolecules* 9 (2008) 2259–2264, <https://doi.org/10.1021/bm800429a>.
- [19] M. Nichifor, M.C. Stanciu, B.C. Simionescu, New cationic hydrophilic and amphiphilic polysaccharides synthesized by one pot procedure, *Carbohydr. Polym.* 82 (2010) 965–975, <https://doi.org/10.1016/j.carbpol.2010.06.027>.
- [20] G. Chen, T. Li, C. Chen, C. Wang, Y. Liu, W. Kong, D. Liu, B. Jiang, S. He, Y. Kuang, L. Hu, A Highly Conductive Cationic Wood Membrane, *Adv. Funct. Mater.* 29 (2019) 1902772, <https://doi.org/10.1002/adfm.201902772>.
- [21] J. Zabielska-Matejuk, A. Stangierska, M. Kot, New Ammonium- and 1,2,4-Triazolium-Based Ionic Liquids for Wood Preservation, *J. Wood Chem. Technol.* 35 (2015) 178–192, <https://doi.org/10.1080/02773813.2014.909852>.
- [22] I. Burgert, E. Cabane, C. Zollfrank, L. Berglund, Bio-inspired functional wood-based materials – hybrids and replicates, *Int. Mater. Rev.* 60 (2015) 431–450, <https://doi.org/10.1179/1743280415Y.0000000009>.
- [23] A. Sánchez-Ferrer, J. Guerrero Parra, Exploring Wood as a Sustainable Solution for Water Filtration: Nanoparticle Removal, Size Exclusion and Molecular Adsorption, *Wood Sci. Technol.* (2024).
- [24] M. Jiao, Y. Yao, C. Chen, B. Jiang, G. Pastel, Z. Lin, Q. Wu, M. Cui, S. He, L. Hu, Highly Efficient Water Treatment via a Wood-Based and Reusable Filter, *ACS Mater. Lett.* 2 (2020) 430–437, <https://doi.org/10.1021/acsmaterlett.9b00488>.
- [25] S. Dharmalingam, V. Kugarajah, V. Elumalai, Proton exchange membrane for microbial fuel cells, in: *PEM Fuel Cells*, Elsevier, 2022: pp. 25–53. <https://doi.org/10.1016/B978-0-12-823708-3.00011-0>.
- [26] M. Lei, Q. Zhang, M. Chi, Y. Yu, H. Jiang, S. Wang, D. Min, Anion Exchange membrane with High hydroxide ion conductivity and robust tensile strength fabricated from quaternary ammonia functionalized *Pinus contorta*, *Dougl. Chip. Ind. Crops Prod.* 166 (2021) 113458, <https://doi.org/10.1016/j.indcrop.2021.113458>.
- [27] T. Yang, B. Pang, M. Zhang, N. Sheng, H. Zhang, K. Zhang, Advanced ion-selective wood membranes: Leveraging aligned cellulose nanofibers for enhanced osmotic energy conversion, *Chem. Eng. J.* 496 (2024) 153891, <https://doi.org/10.1016/j.cej.2024.153891>.

- [28] Q. Wu, C. Wang, R. Wang, C. Chen, J. Gao, J. Dai, D. Liu, Z. Lin, L. Hu, Salinity-Gradient Power Generation with Ionized Wood Membranes, *Adv. Energy Mater.* 10 (2020), <https://doi.org/10.1002/aenm.201902590>.
- [29] S. Perveen, S.G. Hussain, M.J. Ahmed, R. Khawar, T. Bin Siraj, M. Saleem, A Viable and sustainable flat- membrane plate-and-frame module for spent acid regeneration and metal ion recovery, *Heliyon* 9 (2023) e18344.
- [30] F. Karas, J. Hnát, M. Paidar, J. Schauer, K. Bouzek, Determination of the ion-exchange capacity of anion-selective membranes, *Int. J. Hydrogen Energy* 39 (2014) 5054–5062, <https://doi.org/10.1016/j.ijhydene.2014.01.074>.
- [31] K. Charlet, F. Saulnier, M. Dubois, A. Béakou, Improvement of wood polymer composite mechanical properties by direct fluorination, *Mater. Des.* 74 (2015) 61–66, <https://doi.org/10.1016/j.matdes.2015.02.012>.
- [32] N.Z. Misak, Langmuir isotherm and its application in ion-exchange reactions, *React. Polym.* 21 (1993) 53–64, [https://doi.org/10.1016/0923-1137\(93\)90054-J](https://doi.org/10.1016/0923-1137(93)90054-J).
- [33] K. Van Aken, L. Strekowski, L. Patiny, EcoScale, a semi-quantitative tool to select an organic preparation based on economical and ecological parameters, *Beilstein J. Org. Chem.* 2 (2006), <https://doi.org/10.1186/1860-5397-2-3>.
- [34] J.D. McClure, Glycidyltrimethylammonium chloride and related compounds, *J. Org. Chem.* 35 (1970) 2059–2061, <https://doi.org/10.1021/jo00831a093>.
- [35] T. Sata, Y. Mizutani, Modification of properties of ion exchange membranes. VI. Electroalytic transport properties of cation exchange membranes with a electrodeposition layer of cationic polyelectrolytes, *J. Polym. Sci. Polym. Chem. Ed.* 17 (1979) 1199–1213, <https://doi.org/10.1002/pol.1979.170170423>.
- [36] R.A. Ghostine, M.Z. Markarian, J.B. Schlenoff, Asymmetric Growth in Polyelectrolyte Multilayers, *J. Am. Chem. Soc.* 135 (2013) 7636–7646, <https://doi.org/10.1021/ja401318m>.
- [37] X.-X. Ye, W. Luo, L. Lin, Y. Zhang, M. Liu, Quaternized lignin-based dye dispersant: Characterization and performance research, *J. Dispers. Sci. Technol.* 38 (2017) 852–859, <https://doi.org/10.1080/01932691.2016.1207545>.
- [38] P.I.F. Pinto, S. Magina, E. Budjav, P.C.R. Pinto, F. Liebner, D. Evtuguin, Cationization of Eucalyptus Kraft LignoBoost Lignin: Preparation, Properties, and Potential Applications, *Ind. Eng. Chem. Res.* 61 (2022) 3503–3515, <https://doi.org/10.1021/acs.iecr.1c04899>.
- [39] M. Frias, P. Blanchet, A. Bégin-Drolet, J. Triquet, V. Landry, Parametric study of a yellow birch surface impregnation process, *Eur. J. Wood Wood Prod.* 79 (2021) 897–906, <https://doi.org/10.1007/s00107-021-01700-7>.
- [40] I. Andersone, D. Cirule, N. Kurnosova, B. Andersons, E. Kuka, Service properties of pine after combining an impregnation treatment with a thermo-hydro modification process, *Wood, Mater. Sci. Eng.* 18 (2023) 11–18, <https://doi.org/10.1080/17480272.2022.2122869>.
- [41] D.H. Page, A Note on the Cell-Wall Structure of Softwood Tracheids, *Wood Fiber Sci.* 7 (1976) 246–248, <http://swst.metapress.com/content/6XK753844865M826>.
- [42] X. Huang, C.B. Roth, Optimizing the Grafting Density of Tethered Chains to Alter the Local Glass Transition Temperature of Polystyrene near Silica Substrates: The Advantage of Mushroom over Brushes, *ACS Macro Lett.* 7 (2018) 269–274, <https://doi.org/10.1021/acsmacrolett.8b00019>.
- [43] A. Dang, C.M. Hui, R. Ferebee, J. Kubiak, T. Li, K. Matyjaszewski, M.R. Bockstaller, Thermal Properties of Particle Brush Materials: Effect of Polymer Graft Architecture on the Glass Transition Temperature in Polymer- <sc>G</sc>rafted Colloidal Systems, *Macromol. Symp.* 331–332 (2013) 9–16, <https://doi.org/10.1002/masy.201300062>.
- [44] W. Gao, Z. Dang, F. Liu, S. Wang, D. Zhang, M. Yan, Preparation of antistatic epoxy resin coatings based on double comb-like quaternary ammonium salt polymers, *RSC Adv.* 10 (2020) 43523–43532, <https://doi.org/10.1039/D0RA07479A>.
- [45] M.M. Hossain, J. Hou, L. Wu, Q. Ge, X. Liang, A.N. Mondal, T. Xu, Anion exchange membranes with clusters of alkyl ammonium group for mitigating water swelling but not ionic conductivity, *J. Memb. Sci.* 550 (2018) 101–109, <https://doi.org/10.1016/j.memsci.2017.12.062>.
- [46] Ö. Gezici-Koç, S.J.F. Erich, H.P. Huinink, L.G.J. van der Ven, O.C.G. Adan, Bound and free water distribution in wood during water uptake and drying as measured by 1D magnetic resonance imaging, *Cellulose* 24 (2017) 535–553, <https://doi.org/10.1007/s10570-016-1173-x>.
- [47] A. Barbetta, P. Fratzl, T. Zemb, L. Bertinetti, Impregnation and Swelling of Wood with Salts: Ion Specific Kinetics and Thermodynamics Effects, *Adv. Mater. Interfaces* 4 (2017), <https://doi.org/10.1002/admi.201600437>.
- [48] S. Xu, G. Zhang, Y. Zhang, C. Zhao, W. Ma, H. Sun, N. Zhang, L. Zhang, H. Jiang, H. Na, Synthesis and properties of a novel side-chain-type hydroxide exchange membrane for direct methanol fuel cells (DMFCs), accessed 7 May 2023, *J. Power Sources* 209 (2012) 228–235, <https://linkinghub.elsevier.com/retrieve/pii/S0378775312004983>.
- [49] M. Havimo, J. Rikala, J. Sirviö, M. Sipii, Tracheid cross-sectional dimensions in Scots pine (*Pinus sylvestris*) – distributions and comparison with Norway spruce (*Picea abies*), *Silva Fenn.* 43 (2009). <https://doi.org/10.14214/sf.188>.
- [50] S. Jansen, B. Choat, A. Pleters, Morphological variation of intervessel pit membranes and implications to xylem function in angiosperms, *Am. J. Bot.* 96 (2009) 409–419, <https://doi.org/10.3732/ajb.0800248>.
- [51] P.J. Schulte, U.G. Hacke, Solid mechanics of the torus–margo in conifer intratracheid bordered pits, *New Phytol.* 229 (2021) 1431–1439, <https://doi.org/10.1111/nph.16949>.
- [52] Y. Marcus, Ionic radii in aqueous solutions, *Chem. Rev.* 88 (1988) 1475–1498, <https://doi.org/10.1021/cr00090a003>.
- [53] M.Y. Kiriukhin, K.D. Collins, Dynamic hydration numbers for biologically important ions, *Biophys. Chem.* 99 (2002) 155–168, [https://doi.org/10.1016/S0301-4622\(02\)00153-9](https://doi.org/10.1016/S0301-4622(02)00153-9).
- [54] A. Eiberweiser, A. Nazet, G. Hefter, R. Buchner, Ion Hydration and Association in Aqueous Potassium Phosphate Solutions, *J. Phys. Chem. B* 119 (2015) 5270–5281, <https://doi.org/10.1021/acs.jpcc.5b01417>.
- [55] J. Wang, X. Guo, Adsorption isotherm models: Classification, physical meaning, application and solving method, *Chemosphere* 258 (2020) 127279, <https://doi.org/10.1016/j.chemosphere.2020.127279>.
- [56] G. Halsey, H.S. Taylor, The Adsorption of Hydrogen on Tungsten Powders, *J. Chem. Phys.* 15 (1947) 624–630, <https://doi.org/10.1063/1.1746618>.
- [57] S. Azizian, S. Eris, Adsorption isotherms and kinetics, in: 2021: pp. 445–509. <https://doi.org/10.1016/B978-0-12-818805-7.00011-4>.
- [58] F. Foglia, Q. Berrod, A.J. Clancy, K. Smith, G. Gebel, V.G. Sakai, M. Appel, J.-M. Zanutti, M. Tyagi, N. Mahmoudi, T.S. Miller, J.R. Varcoe, A.P. Periasamy, D.J. L. Brett, P.R. Shearing, S. Lyonnard, P.F. McMillan, Disentangling water, ion and polymer dynamics in an anion exchange membrane, *Nat. Mater.* 21 (2022) 555–563, <https://doi.org/10.1038/s41563-022-01197-2>.
- [59] C. Chen, Y.-L.-S. Tse, G.E. Lindberg, C. Knight, G.A. Voth, Hydroxide Solvation and Transport in Anion Exchange Membranes, *J. Am. Chem. Soc.* 138 (2016) 991–1000, <https://doi.org/10.1021/jacs.5b11951>.
- [60] Y. Koga, F. Sebe, K. Nishikawa, Effects of Tetramethyl- and Tetraethylammonium Chloride on H₂O: Calorimetric and Near-Infrared Spectroscopic Study, *J. Phys. Chem. B* 117 (2013) 877–883, <https://doi.org/10.1021/jp3082744>.
- [61] C. Cao, Y. Li, A. Fu, G. Deng, X. Li, Y. Li, X. Qiu, Proposal and application of a novel isothermal model for the thermodynamic study of ion exchange reactions, *Chem. Eng. J.* 489 (2024) 151497, <https://doi.org/10.1016/j.cej.2024.151497>.
- [62] C. Huang, M. Gong, Y. Chui, F. Chan, Mechanical behaviour of wood compressed in radial direction-part I. New method of determining the yield stress of wood on the stress-strain curve, *J. Bioresour. Bioprod.* 5 (2020) 186–195, <https://doi.org/10.1016/j.jobab.2020.07.004>.
- [63] E. Güray, A. Kasal, S. Demirci, E. Ceylan, T. Kuskun, Effects of cross-sectional geometry and force direction on bending strength and modulus of elasticity of some softwood beams, *BioResources* 14 (2019) 9258–9270. <https://doi.org/10.15376/biores.14.4.9258-9270>.
- [64] A. Mautner, T. Kobkeathawin, A. Bismarck, Efficient continuous removal of nitrates from water with cationic cellulose nanopaper membranes, *Resour. Technol.* 3 (2017) 22–28, <https://doi.org/10.1016/j.reffit.2017.01.005>.
- [65] H. Schaqui, A. Mautner, U. Perez de Larraya, N. Pfenninger, P. Tingaut, T. Zimmermann, Cationic cellulose nanofibers from waste pulp residues and their nitrate, fluoride, sulphate and phosphate adsorption properties, *Carbohydr. Polym.* 135 (2016) 334–340, <https://doi.org/10.1016/j.carbpol.2015.08.091>.
- [66] A. Breytus, D. Hasson, R. Semiat, H. Shemer, Removal of nitrate from groundwater by Donnan dialysis, *J. Water Process Eng.* 34 (2020) 101157, <https://doi.org/10.1016/j.jwpe.2020.101157>.
- [67] Q. Gao, C.-Z. Wang, S. Liu, D. Hanigan, S.-T. Liu, H.-Z. Zhao, Ultrafiltration membrane microreactor (MMR) for simultaneous removal of nitrate and phosphate from water, *Chem. Eng. J.* 355 (2019) 238–246, <https://doi.org/10.1016/j.cej.2018.08.137>.
- [68] Y. Gu, Y. Sun, Quaternary phosphonium strong based anion exchangers for the selective adsorption of nitrate, *Chem. Eng. J.* 485 (2024) 149650, <https://doi.org/10.1016/j.cej.2024.149650>.
- [69] S. Liu, J.-W. Liu, H. Wang, Y.-X. Yang, S.-T. Liu, D. Hanigan, H.-Z. Zhao, New Antifouling and Antibacterial Membrane Material for Highly Selective Removal of Nitrate and Phosphate, *Ind. Eng. Chem. Res.* 59 (2020) 12114–12122, <https://doi.org/10.1021/acs.iecr.0c01825>.
- [70] S. Hong, F.S. Cannon, P. Hou, T. Byrne, C. Nieto-Delgado, Adsorptive removal of sulfate from acid mine drainage by polypyrrole modified activated carbons: Effects of polypyrrole deposition protocols and activated carbon source, *Chemosphere* 184 (2017) 429–437, <https://doi.org/10.1016/j.chemosphere.2017.06.019>.
- [71] K. Košutić, I. Novak, L. Sipos, B. Kunst, Removal of sulfates and other inorganics from potable water by nanofiltration membranes of characterized porosity, *Sep. Purif. Technol.* 37 (2004) 177–185, [https://doi.org/10.1016/S1383-5866\(03\)00206-5](https://doi.org/10.1016/S1383-5866(03)00206-5).
- [72] H. Gogoi, T. Leiviskä, J. Rämö, J. Tanskanen, Production of aminated peat from branched polyethylenimine and glycidyltrimethylammonium chloride for sulphate removal from mining water, *Environ. Res.* 175 (2019) 323–334, <https://doi.org/10.1016/j.envres.2019.05.022>.
- [73] A.S. Battah, R.-E.-S. Shohaib, M.G. Abdelwahed, H.A. Ezzeldin, M.E.A. Ali, Removal of phosphate ions from polluted water using a hybrid anion exchanger, *Desalin. Water Treat.* 193 (2020) 152–158, <https://doi.org/10.5004/dwt.2020.25825>.
- [74] X. Duan, C.-W. Wang, T. Wang, X. Xie, X. Zhou, Y. Ye, Removal of Metal Ions in Phosphoric Acid by Electro-Electrodialysis with Cross-Linked Anion-Exchange Membranes, *ACS Omega* 6 (2021) 32417–32430, <https://doi.org/10.1021/acsomega.1c03720>.
- [75] H. Ma, Y. Xue, Y. Zhang, T. Kobayashi, K. Kubota, Y.-Y. Li, Simultaneous nitrogen removal and phosphorus recovery using an anammox expanded reactor operated at 25 °C, *Water Res.* 172 (2020) 115510, <https://doi.org/10.1016/j.watres.2020.115510>.
- [76] F.W. Stull, D.F. Martin, Comparative ease of separation of mixtures of selected nuisance anions (nitrate, nitrite, sulfate, phosphate) using Octolig®, *J. Environ. Sci. Heal. Part A* 44 (2009) 1545–1550, <https://doi.org/10.1080/10934520903263454>.
- [77] M. Escolà Casas, M. Guivernau, M. Viñas, B. Fernández, R. Cáceres, C. Biel, V. Matamoros, Use of wood and cork in biofilters for the simultaneous removal of nitrates and pesticides from groundwater, *Chemosphere* 313 (2023) 137502, <https://doi.org/10.1016/j.chemosphere.2022.137502>.

- [78] J. Jaafar, A.M. Nasir, Grand Challenge in Membrane Fabrication: Membrane Science and Technology, *Front. Membr. Sci. Technol.* 1 (2022) 3, <https://doi.org/10.3389/FRMST.2022.883913>.
- [79] X.T. Le, T.H. Bui, P. Viel, T. Berthelot, S. Palacin, On the structure–properties relationship of the AMV anion exchange membrane, *J. Memb. Sci.* 340 (2009) 133–140, <https://doi.org/10.1016/j.memsci.2009.05.025>.
- [80] B. Lee, A. Jiao, S. Yu, J.B. You, D.-H. Kim, S.G. Im, Initiated chemical vapor deposition of thermoresponsive poly(N-vinylcaprolactam) thin films for cell sheet engineering, *Acta Biomater.* 9 (2013) 7691–7698, <https://doi.org/10.1016/j.actbio.2013.04.049>.
- [81] B. Wang, J. Yan, H. Wang, R. Li, R. Fu, C. Jiang, V. Nikonenko, N. Pismenskaya, Y. Wang, T. Xu, Ionic liquid-based pore-filling anion-exchange membranes enable fast large-sized metallic anion migration in electrodialysis, *J. Memb. Sci.* 670 (2023) 121348, <https://doi.org/10.1016/j.memsci.2023.121348>.
- [82] R.W. Herschy, Water quality for drinking: WHO guidelines, *Encycl. Earth Sci. Ser.* (2012) 876–883, https://doi.org/10.1007/978-1-4020-4410-6_184.
- [83] *Who Who Guidelines for Drinking Water Quality 4th ed.*, 2017 New York.